

## **Response to comments of referee #1**

### **General Comments:**

**Reviewer:** This paper is an analysis of a 4 years data set of aerosol parameters (scattering, backscattering and absorption coefficients, SMPS) measured at Melpitz. First a closure study is performed to compare scattering and backscattering coefficient measurements with the results of a Mie code calculation based on SMPS measurements. Second, the Mie code was used to calculate “true values” of the scattering and backscattering coefficients without the truncation and non-Lambertian error. These results allow to make assumption on the validity of the Anderson and Ogren (1998) algorithm that correct for these two systematic errors. Third, statistical values and seasonal cycles of the aerosol parameters are presented. Finally the variations of the aerosol parameters as a function of air masses origins are analyzed.

The paper presents a worthy 4-years dataset and some interesting analysis. There is however different points that have to be revised:

### **Response:**

*Thanks for the referee's comments. We have improved our work according to the referee's comments and suggestions.*

### **Major Comment 1**

#### **Reviewer:**

- Air mass classification: it is first quite difficult to obtain an idea of the classification scheme presented, since the publication about it is planned in a forthcoming paper.

#### **Response:**

*We agree that it this is indeed not a perfect situation because the work on the new classification is still ongoing. Nevertheless, we see so many advantages of this new classification that we prefer to use it for this publication. In order to improve the understanding of that new scheme we supply, in the revised version of the current paper, more extended information about this classification is given.*

*The text in Sect. 2.3, for example, was extended as follows:*

*“The back trajectory cluster method (BCLM) is explained in detail in the following. BCLM is based on a joint cluster analysis of daily backtrajectories and profiles of pseudopotential temperature obtained from radiosoundings (Engler et al., 2007; Birmili et al., 2010). Pseudopotential temperature is included in the method because it is an essential indicator on whether the boundary layer can be considered mixed or not during daytime. Technically, the cluster algorithm belongs to the family of k-means cluster algorithms. Our modified method, used for the first time here, uses extended functionality in that it processes simultaneously backtrajectories started at nine locations spread over Germany, and on radiosoundings measured at seven locations. The cluster algorithm thus yields air mass types that are representative for entire Germany. 3D-backward trajectories were calculated using a PC version of HYSPLIT, a trajectory model provided by the NOAA Air Resources Laboratory (Draxler and Hess, 2004). Back trajectories were calculated from the Global Data Assimilation System (GDAS) analysis set, which provides meteorological fields every 3 h, a spatial horizontal resolution of 1°, and a vertical resolution corresponding to the standard pressure levels (1000, 925, 850 hPa, etc.). Backward trajectories starting at 12:00 UTC and reaching 96 h back in time were computed for a starting level of 500 m above the ground. Radio soundings were started daily at 12:00 UTC at seven meteorological stations in Germany. Due to the gradual evolution of the mixed layer during the day, the latter measurements will strongly indicate*

*whether the boundary layer is well-mixed on a particular day or not. To make the vertical profiles comparable throughout all seasons, all profiles were normalized to 0°C at a height of 100 m above ground.”*

**Reviewer:**

Second, there is already several synoptic weather classification schemes over Germany and Europe (see for ex the final report of the Cost 733 action: <http://cost733.met.no/FinalEvent.html>), which were tested and used in several studies. It would be worth to use an already well-known and accepted classification scheme instead of developing a new one.

**Response:**

*We agree with you that indeed a number of other weather classification schemes have been available. To pick up your suggestion, we compared our present back trajectory cluster analysis with two other, freely available weather classification schemes from the Cost 733 action: 1) The Hess and Brezowsky Grosswetterlagen scheme (Cost No. 1, “HBGWL”, Hess and Brezowsky, 1952), and 2) Objective weather classification (Cost No. 19, “WLKC09”, Dittmann, 1995). Both schemes are already optimised in that they focus on Central Europe as a target region. We applied these schemes to our data set, showing the corresponding results in the supplementary material at the bottom of this letter. As we could see, the predictive power of these two classification schemes does not match that of our present back trajectory cluster analysis.*

*We therefore prefer to keep the presentation of results based on the existing scheme. Concretely, we changed the text in Sec. 2.3 as follows:*

*“To attribute the measured optical aerosol properties to specific air mass types, we divided the experimental data set according to several air mass classification schemes. The first scheme is a recently developed air mass classification scheme for surface-level tropospheric aerosols, and involves a clustering of numerical back trajectories and measured profiles of pseudo-potential temperature (denoted back trajectory cluster method, BCLM, hereafter). The usefulness of this classification has been demonstrated in several previous works (Engler et al., 2007; Birmili et al., 2010; Heintzenberg et al., 2011). The second and third schemes are established classification schemes that have taken part in comparisons of the Cost 733 action (Philipp et al., 2010): The Hess and Brezowsky Grosswetterlagen scheme (Cost No. 1, “HBGWL”, Hess and Brezowsky, 1952), and Objective Weather Classification (Cost No. 19, “WLKC09”, Dittmann, 1995). These two schemes are described in more detail in the supplementary material. With respect to the segregation of aerosol optical measurements at Melpitz, the latter two classification schemes turned out to be less useful than the BCLM method. Therefore, their corresponding results are only shown in the supplementary material.”*

**Reviewer:**

The resulting 13 air mass types are not completely self-explaining. Several questions remain open: what are the cold/warm season?

**Response:**

*In our classification, the tendency of vertical mixing is expressed by the vertical profile of pseudo-potential temperature recorded at 12:00 UTC (= 13:00 local time). In fact, this criterion is so strong that it will almost naturally split the days into periods of more and less stable stratification. In practice, days with less stable stratification occur much more frequent in the cold season (~ winter) while days with more stable stratification occur more frequent in the warm season (~ summer).*

*To answer your question: the real underlying criterion for classification is the vertical temperature profile, and not the question whether a day strictly fell into winter or summer.*

However, since appeared somewhat unspecific, particularly to non-meteorologists, we labelled the clusters after “cold season – CS” and the “warm season – WS”.

The final paragraph in Sect. 2.3. was reformulated to clarify this issue.

**Reviewer:**

How is the evolution of the mixed layer defined?

**Response:**

The tendency of an air mass for vertical mixing is expressed by the vertical profile of pseudo-potential temperature, as recorded from the 12:00 UTC (= 13:00 local time) radiosounding. This aspect is now much better explained, and vertical profiles of pseudo-potential temperature are now supplied as an additional Figure 2 in the manuscript, as shown follows:

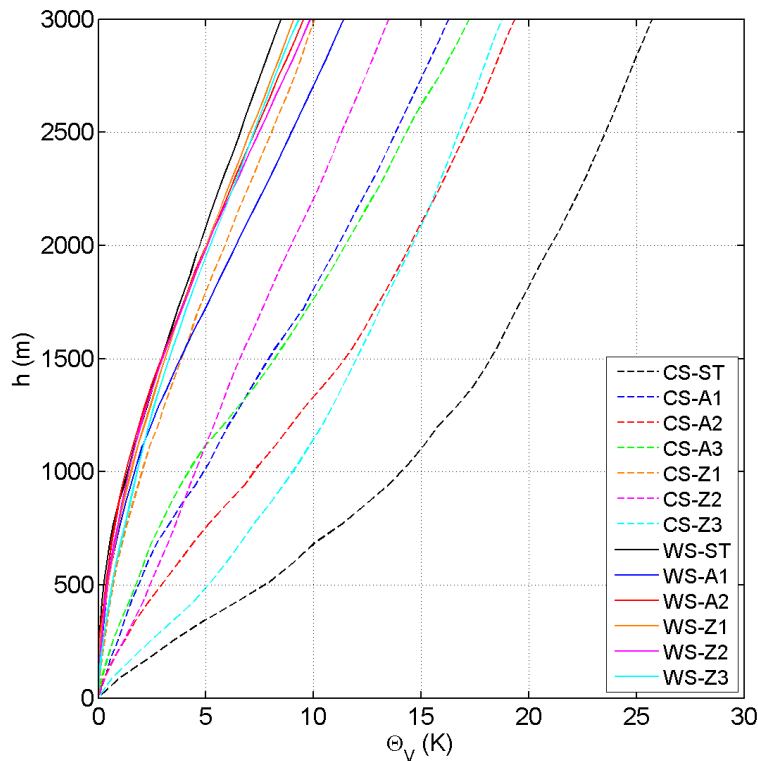


Figure 2. Average normalized profiles of pseudopotential temperature ( $\theta_v$ ) for the 13 air mass types reported. Profiles with a flat gradient indicate a temperature inversion. Profiles with a steep gradient imply stratification close to neutral. Data originate from the radiosoundings launched at the DWD station Lindenberg, located 115 km northeast of Melpitz.

**Reviewer:**

What is the effect of the normalization of the vertical profiles (which ones, P, T, humidity, wind?)?

**Response:**

Normalisation is made to the vertical profile of pseudo-potential temperature exclusively. The profiles are normalised so that they are 0°C at 100 m above the ground. This will make cold season and warm season profiles comparable. (A level 100 m above the ground is chosen to avoid the effects of local overheating of the surface, as could be seen in the profiles on individual days.) The motivation is that stratification is what matters for pollution dispersal, not absolute temperature. A new Figure 2 is introduced that makes this more understandable.

## Major Comment 2

### Reviewer:

- The authors have used SMPS measurements associated with Mie codes to obtain the closure study. Other assumptions given later in the paper could be tested/explained by SMPS results and Mie codes, but the authors prefer to cite other papers or rely on global explanations. Here are several examples: 1) each time where primary or secondary aerosol production are taken as an argument, SMPS could help to show the relation between, for example, the lower single scattering albedo in winter and the secondary aerosol production (p. 27827). 2) the relation between  $b$  and the decrease in aerosol mean size (p. 27827) 3) the difference of the seasonal cycles of the scattering Ångström exponents calculated with different pairs of wavelengths (Fig. 4)

### Response:

*Thanks for this suggestion. According to this issue, a number of revisions have been made in section 3.4, 3.5 and 3.6, trying to interpret the results based on measured aerosol number size distribution and Mie mode results. The annual variation of aerosol total number concentration and the effective radius of submicron aerosol was added in fig. 5:*

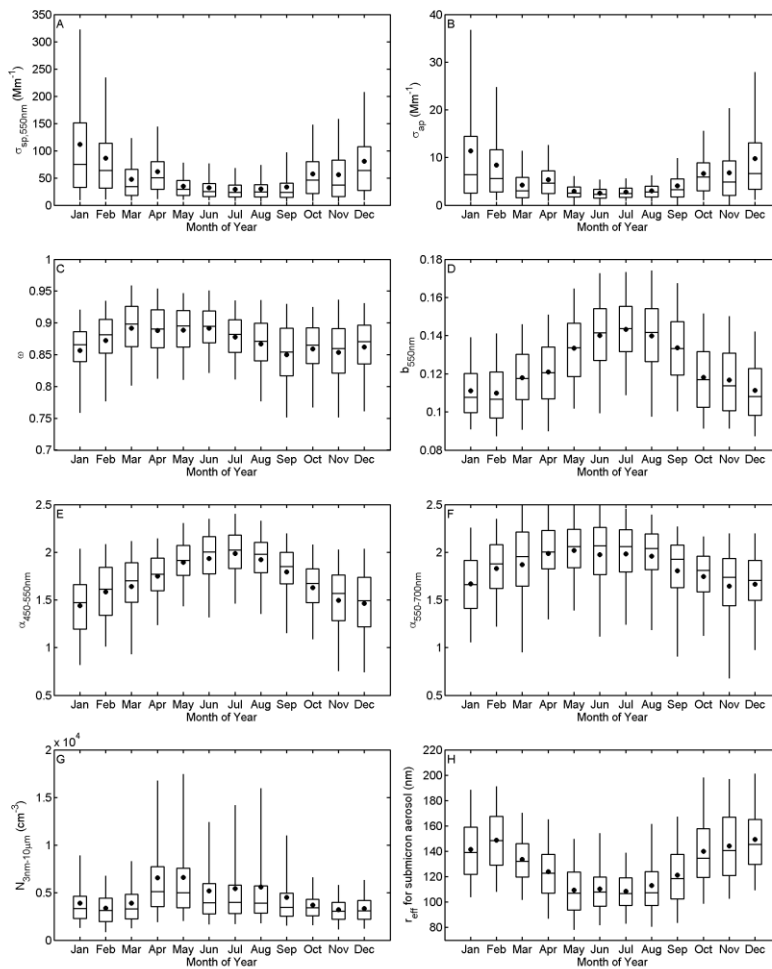


*Figure 5. Annual variations of aerosol scattering coefficient (A), absorption coefficient (B), single scattering albedo (C), hemispheric backscattering fraction (D), Ångström exponent at 450-550 nm (E) and at 550-700 nm (F), aerosol total number concentration (G), and the effective radius of submicron aerosol.*

For each panel, the boxes and whiskers denote the 5, 25, 50, 75 and 95 percentiles, while the dots denote the mean values.

And 3 new figures have been added in the manuscript. For example, when explain the annual variation of  $\omega$  in section 3.4:

“Figure 6 shows the average diurnal variation of aerosol number size distribution in the four seasons, based on the measurements of TDMPS and APS from 2008 to 2010. It can be seen that new particle formation and the consequent growth of nucleation mode particles are evident in daytime in spring and summer. In these two seasons, secondary aerosol productions via photochemistry processes are efficient and results in a large fraction of non-light-absorbing components such as organic matter and sulfate in particulate matters (Poulain et al., 2011), hence yielding a relatively higher level of  $\omega$ . The “banana shape” can not be easily seen in fall and disappeared in winter, indicating the inhibition of secondary aerosol production in these two seasons, thus resulting in a relatively lower level of  $\omega$ .”

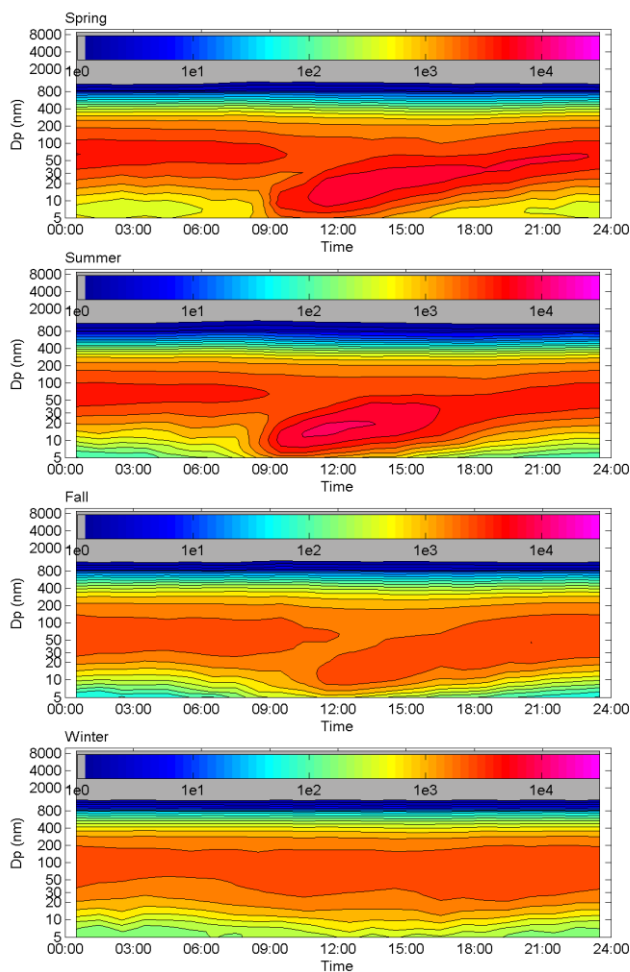


Figure 6. Average diurnal variation of aerosol number size distribution in the four seasons, based on the measurements of TDMPS and APS from 2008 to 2010.

Another example, in the discussion of the annual pattern of  $b$ :

“Evident annual cycle can be found in  $b$ , with higher values in summer than in winter. This annual pattern can be attributed to the variation of both the number size distribution and the mixing state of particles. As

mentioned above, due to the secondary aerosol formation in spring and summer, a significant nucleation mode can be usually found and causes a decrease of the effective radius of submicron aerosol. As shown in fig. 10(D), there is a significant inverse correlation between  $b$  and the effective radius of submicron aerosol. The low level of the effective radius of submicron aerosol therefore results in a high level of  $b$  in summer.”

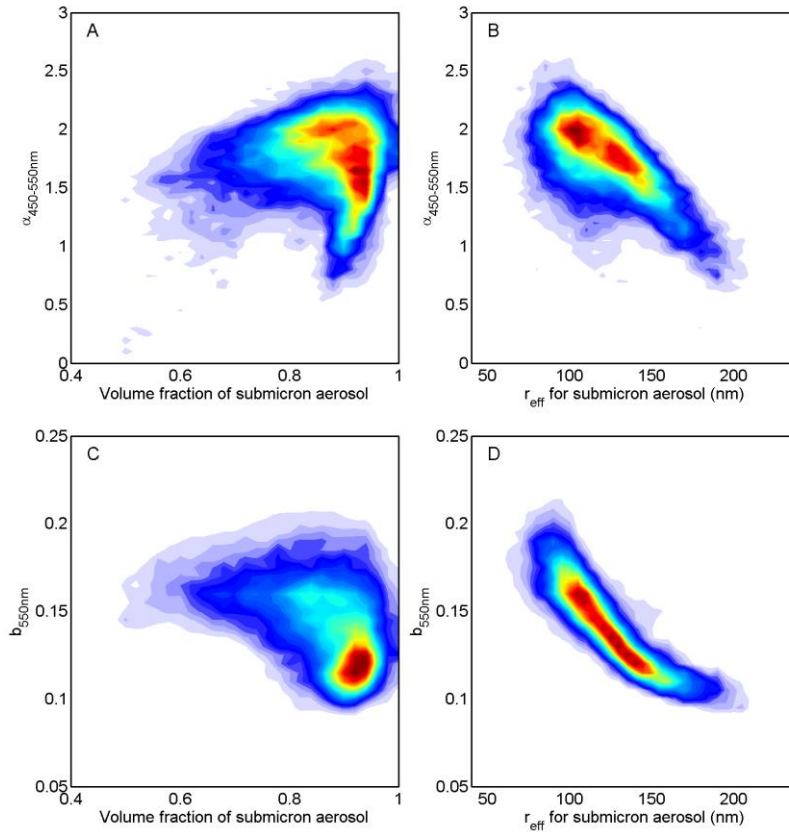


Figure 10. Correlation between  $\alpha$  and volume fraction of submicron aerosol(A),  $\alpha$  and effective radius of submicron aerosol (B),  $b$  and volume fraction of submicron aerosol (C),  $b$  and effective radius of submicron aerosol (D). To visualize the data distribution, the counts of data points are displayed as an intensity graph.

And another example, in the explanation of the difference of the seasonal cycles of the scattering Angström exponents calculated with different pairs of wavelengths:

“One should also note that the  $\alpha$  for the two wavelength pairs show some difference in their annual patterns.  $\alpha_{450-550nm}$  in summer is at the similar level as  $\alpha_{550-700nm}$ , while in winter  $\alpha_{450-550nm}$  is lower than  $\alpha_{550-700nm}$ .  $\alpha_{450-550nm}$  therefore shows a more obvious annual variation compared with  $\alpha_{550-700nm}$ . This is because the  $\alpha$  for different wavelength pairs has different response on the variation of aerosol number size distribution. Figure 7 shows the measured  $\alpha_{450-550nm}$  and  $\alpha_{550-700nm}$  versus the corresponding effective radius of submicron aerosol. It can be found that  $\alpha_{450-550nm}$  is more sensitive to the variation of the effective radius of submicron aerosol than  $\alpha_{550-700nm}$ . With the increase of the effective radius of submicron aerosol,  $\alpha_{450-550nm}$  decrease with a steeper slope than  $\alpha_{550-700nm}$ . In the cases of  $r_{eff}$  lower than 120 nm (i.e. in summer), the two  $\alpha$  are in the similar level; while in the case of  $r_{eff}$  higher than 140 nm (i.e. in winter),  $\alpha_{450-550nm}$  is lower than  $\alpha_{550-700nm}$ .”

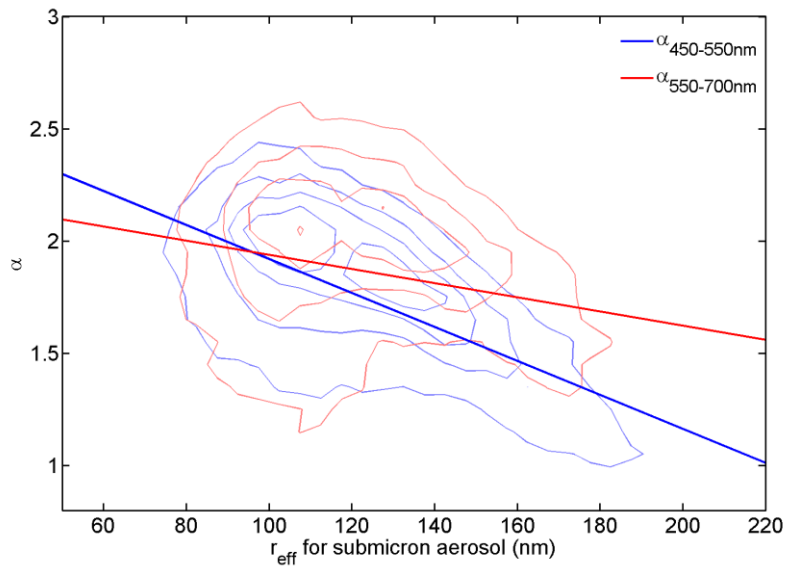


Figure 7. Measured  $\alpha_{450-550\text{nm}}$  and  $\alpha_{550-700\text{nm}}$  versus the corresponding effective radius of submicron aerosol in the period of 2008-2010. To visualize the data distribution, the counts of data points are displayed as contour graphs. The red and blue straight lines represent the linear regression fits to the data.

More examples for this issue are shown in the response of minor comment 14, 16, 17, 18, 19, and the response of the general comment of reviewer#2.

### **Major Comment 3**

#### **Reviewer:**

- Generally the choice of the figures is not appropriate: some assumption could be validated by making correlation between different parameters (for ex. between  $b$  and the effective radius of sub-micron aerosol or their volume fraction), whereas several figures does not bring a lot of informations (Fig. 1 and 3)

#### **Response:**

*Thanks for this comment. Following the reviewer's suggestion, almost all the figures in the manuscript have been revised. Figure 1 and 3 was deleted. Seven other new figures were added. Figure 6 and 7 has been merged together. The list of all the figures in the revised manuscript is shown as an appendix in the bottom of this response.*

### **Minor comments:**

#### **1. Reviewer:**

- p. 27812 line 6: specify that you are speaking of the scattering Angström exponent

#### **Response:**

*Thanks for the correction. All the "Ångström exponent" in the manuscript has been change to "scattering Ångström exponent".*

#### **2. Reviewer:**

- p. 27813: update your results with the IPCC 2013 report

**Response:**

*The corresponding sentence has been revised as:*

*“The effective radiative forcing caused by these two effects is estimated as  $-0.45 \text{ Wm}^{-2}$  and  $-0.45 \text{ Wm}^{-2}$ , respectively, with their uncertainties being the largest among all climate forcing factors (IPCC, 2013).”*

**3. Reviewer:**

- p. 27813 and 27825: I do not agree at all that only seldom studies have been published on at least one year of aerosol optical measurements. See first the ebas data base listing the data regularly submitted or the recent papers on long-term trend analysis of aerosol optical properties and number concentration (Asmi et al., ACP 2013, Collaud Coen et al., ACP 2013) that obtain more than 20 datasets with more than 10 years of measurements. There is certainly a lot of publications involving all these datasets.

**Response:**

*Thanks for correcting this mistake. The sentence “Long term in-situ observations of aerosol optical properties (i.e. longer than one year) have seldom been reported, and no such observations have been described for the Central European troposphere.” in p.27813 has been revised as:*

*“There have been a number of studies reporting long term (i.e. longer than one year) in-situ measurements of aerosol optical properties (e.g. references in Asmi et al., 2013, and references listed in table 8). However, none of them describes for the regional background troposphere on Central European Plain.”*

*The sentence “Only a few published studies reported continuous measurements of aerosol scattering and absorption properties with an observation period longer than 1 yr.” in p. 27825 has been deleted.*

*We have also selected some results from these long term studies for the comparison of single scattering albedo, as shown in the response for comment 10.*

**4. Reviewer:**

- §2.2: it is not clear is the truncation and non-lambertian error correction were applied to the scattering and backscattering coefficients before the closure or not

**Response:**

*Actually the optical closure study was conducted for the direct output of the TSI 3563 nephelometer, with a modified Mie model which including the two measurement errors. The correction was applied afterwards based on the Mie calculations in the closure study. A sentence has been added in the first paragraph of section 3.1 to make it clearer:*

*“The optical closure was conducted before the correction of the truncation and non-Lambertian error of nephelometer measurement. The correction was applied based on the Mie calculations introduced in Sect. 2.2 afterwards.”*

**5. Reviewer:**

-p. 27821: the uncertainties were set according to Ma et al., (2011) dealing with aerosol measurements in China: are the aerosol types and the instruments used in both studies sufficiently comparable to have the same uncertainties?

**Response:**

*The uncertainties of the measured particle number size distributions and light-absorbing carbon mass concentrations are mainly determined by the design of instruments. The uncertainties used in Ma et al. (2011) were set according to test reports of instruments (e.g. Wiedensohler et al., 2010; Petzold et al.,*

2004). Therefore, with the exactly same instrumentation, we used the same setting of uncertainties. To avoid misunderstanding, the reference has been changed to the original literatures:

*“The uncertainties of the measured particle number size distributions and light-absorbing carbon mass concentrations ( $m_{LAC,MAAP}$ ) were set according to Wiedensohler et al. (2012), Wex et al. (2002) and Petzold et al. (2004), as shown in table 3.”*

#### **6. Reviewer:**

-p. 27822 §3.1.3: please use the same structure of sentences to explain how are estimated the boundary of the scattering and the backscattering.

#### **Response:**

*The treatment for  $\sigma_{sp}$  and  $\sigma_{bsp}$  were exactly the same. Therefore we concentrated the explanation into one sentence:*

*“For  $\sigma_{sp}$  and  $\sigma_{bsp}$ , the calculated values with external mixture assumption plus triple standard deviation and the calculated values with core-shell internal mixture assumption minus triple standard deviation were considered as the boundaries of the possible range within which the measured values should fall.”*

#### **7. Reviewer:**

-p. 27822: in my opinion, the stability of the measurement cannot be estimated by the presented closure study. The stability has to be tested as a function of time and not only as a percentage of measured data explained by the closure study. For me also, the aim of a closure study does not seems to be the validation of the measurements.

#### **Response:**

*We agree with the reviewer that a closure is not a tool for testing the stability of measurements. Testing the stability requires stable aerosol conditions, what we never will find in the atmosphere. But if the closure is fulfilled over a long time period, it can show that the instruments were not drifting too much. Therefore, we replace the sentence “...confirming a stable performance of the instruments and a good quality of the data set.” with “...confirming that there is not obvious large, unacceptable drift of instruments, as well as a good quality of the data set.”*

*We do not fully agree to the reviewer that the aim of a closure study is not a validation of the measurements. Validation of measurements can be one goal of a closure. In modern experiments a closure is usually used to derive more parameters, e.g. the refractive index. But then we rely on the fact that the instruments are all ok. If the closure shows strange results, for example, the retrieved refractive index is far from reasonable values, we can claim that the measurements are probably wrong. In that sense a closure is always a validation of measurements.*

#### **8. Reviewer:**

-p. 27823: the difference between the regular and modified Mie model is not explained

#### **Response:**

*Thanks for the comment. To explain the difference between the modified and regular Mie model, text shown below has been added in section 2.2:*

*“To simulate the measurements of TSI 3563 nephelometer, a modified BHMIE code and a modified BHCOAT code (Bohren and Huffman, 1983; Cheng et al., 2009) were used for homogeneous spherical particles and core-shell mixed spherical particles, respectively.*

In the Mie theory (Mie, 1908), the scattering efficiency  $Q_{sp}$  and hemispheric back scattering efficiency  $Q_{bsp}$  can be calculated by integrating the scattering intensity function  $|S(\theta, x, \tilde{m})|$  from  $0^\circ$  to  $180^\circ$  and from  $90^\circ$  to  $180^\circ$ , respectively:

$$Q_{sp,bsp} = \frac{1}{x^2} \int_{\theta} |S(\theta, x, \tilde{m})|^2 \sin \theta d\theta \quad (1)$$

where,  $x = \pi D_p / \lambda$ .  $D_p$  is the volume equivalent diameter of particles.  $\lambda$  is the wavelength of light, and  $\theta$  is the scattering angle.

Different from the regular scattering angle ranges mentioned above, the scattering integration angle of TSI 3563 nephelometer ranges from  $7^\circ$  to  $170^\circ$  for scattering and from  $90^\circ$  to  $170^\circ$  for hemispheric back scattering, respectively. Thus, the measured values are truncated in the near-forward and near-backward angular ranges. Furthermore, the light source of nephelometer is not strictly Lambertian and shows a non-ideal angular response (Anderson et al., 1996). The angular response is solved in the Mie calculations based on the BHMIE and BHCOAT code (Bohren and Huffman, 1983). The  $\sin \theta$  term in equation (1) is replaced by the angular sensitivity curves  $f(\theta)_{sp}$  and  $f(\theta)_{bsp}$ , derived from a calibration experiment of the TSI 3563 nephelometer (Anderson et al., 1996). The  $\sigma_{sp}$  and  $\sigma_{bsp}$  are calculated as:

$$\sigma_{sp,bsp} = \int_{D_p} \left[ \frac{1}{x^2} \int_{\theta} |S(\theta, x, \tilde{m})|^2 f(\theta)_{sp,bsp} d\theta \right] \cdot \left( \frac{\pi}{4} D_p^2 \right) \cdot N(\log D_p) \cdot d \log D_p \quad (2)$$

Where,  $N(\log D_p)$  is the aerosol number size distribution.”

## 9. Reviewer:

-§3.2: this study seems to me the most interesting point of the paper. It should be however compared to the results at other sites. The measurements were done with a PM10 inlet. What is the influence of the size cut on the results of Fig. 2?

## Response:

Following the reviewer’s suggestion, we calculated  $C_{sp}$  based on 1-year measurement of aerosol number size distribution in a suburban station Leipzig-TROPOS, and discussed the reason of the mismatch between  $C_{sp}$  calculated with Mie model and Anderson’s method. We also gave some suggestions in which case Anderson’s method is not applicable. One figure and several paragraphs have been added in the manuscript, as follows:

“To better understand the mismatch between the  $C_{sp}$  yielded from Anderson’s parameterization and Mie calculation,  $C_{sp}$  was calculated based on aerosol number size distribution measured in another station, Leipzig-TROPOS, from 2010.1.1 to 2010.12.31. Leipzig-TROPOS is a suburban station representative of the urban background aerosol, which is also a part of network GUAN (German Ultrafine Aerosol Network; Birmili et al., 2009). With the same instrumentation, the measured data was processed according to section 2.1, and 1-hour data was used. The  $C_{sp}$  was then calculated with each individual aerosol size distribution with the same method which applied for Melpitz data. Figure 4(B) shows the calculated  $C_{sp}$  at 550 nm versus  $\alpha$ . The color of data points denotes the volume fraction of submicron aerosol ( $f_{V-submicron}$ ) calculated with corresponding aerosol size distribution. As a comparison, the results of Melpitz in the same time period are also shown in fig. 4(A). It can be found in fig. 4 that the locations of the data points strongly depend on  $f_{V-submicron}$ . The points for both Melpitz and Leipzig-TROPOS are close

to the submicron case in Anderson's method (black dash line) if  $f_{V\text{-submicron}}$  is larger than 0.8. And the points in Leipzig-TROPOS follow well with the no-cut case in Anderson's method (the black solid line) for case of  $f_{V\text{-submicron}}$  smaller than 0.7.

The  $C_{sp}$  mainly depends on the corresponding aerosol number size distribution. In Anderson et al. (1998), they assumed a series of bimodal log-normal aerosol number size distributions, with geometric mean diameter set within 200-400 nm and 2-4  $\mu\text{m}$  for the two modes, respectively. These generated aerosol number size distributions were then used for calculating  $C_{sp}$  with Mie model. And the parameters  $a_1$  and  $a_2$  were determined by linear fits of  $C_{sp}$ . However, these assumed bimodal log-normal distributions may not be representative of the aerosol in the region of our measurement. Due to the active secondary production and anthropogenic emission in the region, aerosol optical properties are dominated by the submicron aerosol in Melpitz. Figure 4(C) shows the relative frequency distribution of  $f_{V\text{-submicron}}$ . It can be seen that submicron aerosol takes more than 70% of the total aerosol volume in most cases in Melpitz. And  $f_{V\text{-submicron}}$  is never below 50%. Therefore, with the domination of submicron aerosol, the correlation between  $C_{sp}$  and  $\alpha$  is similar with submicron case rather than no-cut case in Anderson's method. In Leipzig-TROPOS, the frequency distribution of  $f_{V\text{-submicron}}$  is broader than in Melpitz. There are a number of cases with  $f_{V\text{-submicron}}$  lower than 70%. For these cases, the correlation between  $C_{sp}$  and  $\alpha$  match well with the no-cut case in Anderson's method.

Therefore, if the aerosol volume concentration is always dominated by submicron aerosol, as the case of Melpitz, the method developed by Anderson et al. (1998) is applicable with new parameters  $a_1$  and  $a_2$ . However, if the volume concentration is sometimes also dominated by coarse aerosol, as the case of Leipzig-TROPOS, it is impossible to use  $C_{sp} = a_1 + a_2 \cdot \alpha$  to fit all the data points well. As shown in fig. 4(B), the fit result is not representative of the data points, and the  $R^2$  is only 0.452. The only solution for this case is calculating  $C_{sp}$  with Mie model and aerosol number size distribution measured parallel."

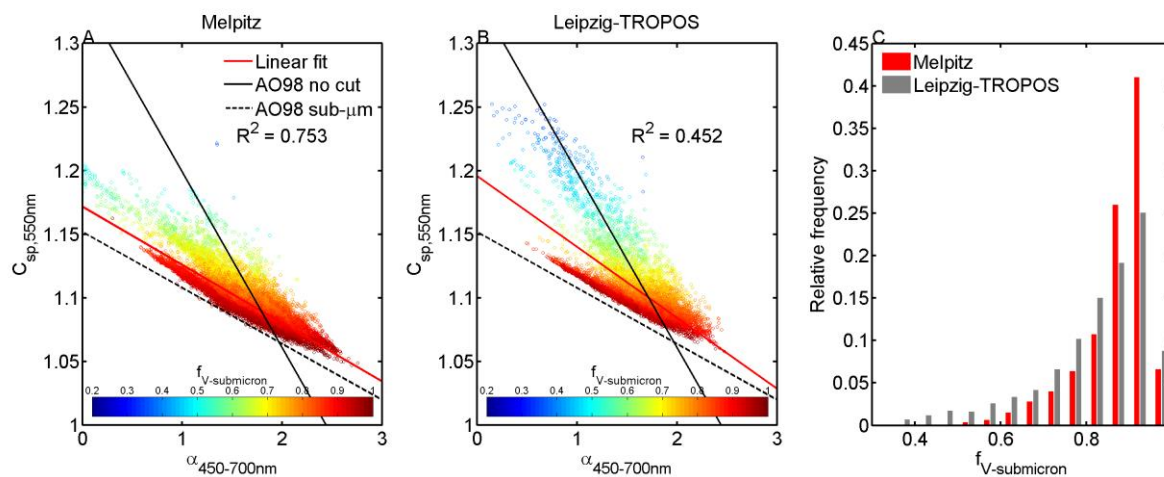


Figure 4. Correlation between calculated  $C_{sp}$  and measured  $\alpha_{450-700\text{nm}}$  at Melpitz (A) and Leipzig-TROPOS (B). Colors of dots denote the corresponding volume fraction of submicron aerosol to total aerosol. The red straight lines represent the linear regression fits to the data. (C) The relative frequency distribution of the volume fraction of submicron aerosol in Melpitz and Leipzig-TROPOS.

Using a PM10 inlet, what we measured is actually not the whole aerosol population. However, without extremely cases like heavy dust event, the optical contribution of particles larger than 10  $\mu\text{m}$  is negligible.

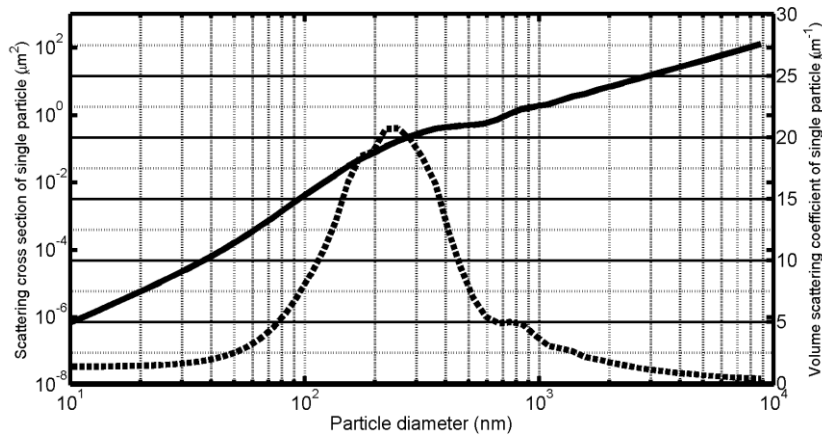


Figure R1. single-particle scattering cross section (solid line) and the single-particle scattering cross section divided by particle volume (dash line; named volume scattering coefficient of single particle) for different particle diameter.

Figure R1 shows the single-particle scattering cross section and the single-particle scattering cross section divided by particle volume (named volume scattering coefficient of single particle) for different particle diameter, calculated with Mie mode assuming a refractive index of 1.55-0.03i. It can be seen that although the scattering cross section significantly increases monotonically with the increase of particle size. The volume scattering coefficient of single particle shows an evident unimodal pattern, with a maximum located between 200 and 300 nm. The values decrease with the increase of particle size for particles larger than 1  $\mu\text{m}$ , and are very close to 0 for diameter of 10  $\mu\text{m}$ .

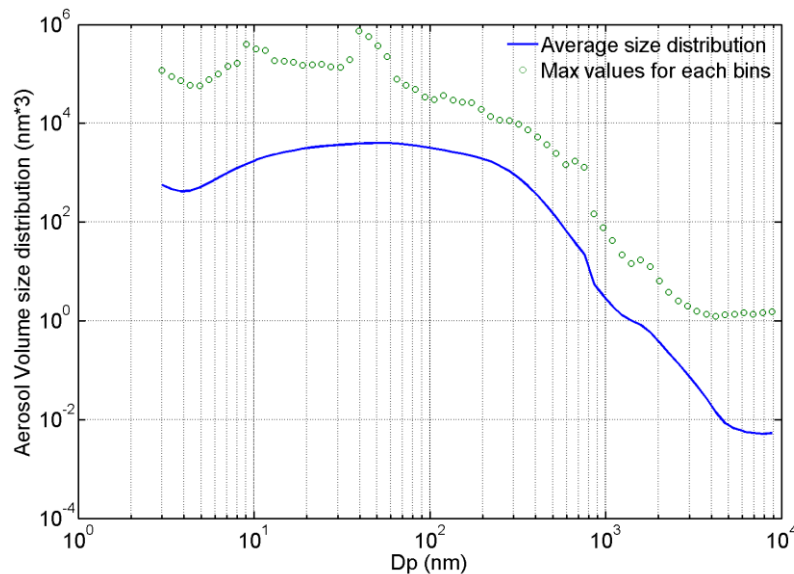


Figure R2. the average aerosol volume size distribution in Melpitz. Green dots show the maximum values of each size bin.

On the other hand, the volume concentration also decreases with the increase of particle size for particles larger than 1  $\mu\text{m}$ . Figure R2 shows the average aerosol volume size distribution in Melpitz, as well as the maximum values of each size bin. It can be seen that even the maximum values for particles larger than 5  $\mu\text{m}$  are still very low comparing with submicron particle. With negligible single particle volume scattering

coefficient and low volume concentration, the optical contribution of particles larger than 10  $\mu\text{m}$  is assumed to be negligible.

#### 10. Reviewer:

- §3.3: Fig. 3, 4 and tables 7 and 8 are somewhat redundant. The comparison with mean values found at other stations does not bring a lot of informations since it is quite difficult to estimate if these aerosol measured at these station are comparable. For example, what is the meaning of Finokalia (marine station) scattering coefficient being 10% higher than at Melpitz? Moreover, there is a lot of papers published of the time series of Puy du Dôme, Hohenpeissenberg, Jungfraujoch, Cabauw, Mace Head, Sonnblick, Ispra, K-Puzta... The comparison of the single scattering albedo would have been more valuable.

#### Response:

*Thanks for this comment. As the reviewer said, figure 3, 4 and table 8 bring basically similar information. Therefore, we decided to delete figure 3 and table 8. Figure 4 and table 7 are kept to show the seasonal variations and the overall statistics.*

*We agree with the reviewer that “the comparison with mean values found at other stations does not bring a lot of informations since it is quite difficult to estimate if these aerosol measured at these station are comparable”. The average  $\sigma_{sp}$  and  $\sigma_{ap}$  strongly depend on the type of the measurement station (e.g. urban, rural, mountain, marine...). Comparison between stations of different types does not bring much information. We have deleted most of the comparison for  $\sigma_{sp}$  and  $\sigma_{ap}$  in section 3.3, and only selected two sites for the comparison: SDZ and SGP, which are respectively representative of continental regional aerosol in the North China and Middle America.*

*As suggested by the reviewer, we add a table of  $\omega$  obtained in other long-term in-situ measurement around the world, as well as some discussion in section 3.3, as shown below:*

*“It should be noted that the  $\sigma_{sp}$  and  $\sigma_{ap}$  at Melpitz was measured at relatively dry conditions ( $RH < 40\%$ ). The ambient  $\omega$  may be higher due to the hygroscopic growth of aerosol. As an intensive aerosol property which is important for aerosol direct radiative forcing, it is valuable to compare the  $\omega$  in Melpitz with those measured in other regionals. Table 8 lists the average  $\omega$  obtained in other long-term in-situ measurement around the world. With different instrumentation, the  $\omega$  was provided at different wavelengths in different studies. To compare  $\omega$  calculated at different wavelengths, the average  $\omega$  in Melpitz was adjusted to several wavelengths based on the average scattering Ångström exponent listed in table 7 and an absorption Ångström exponent of -1, as shown in table 8. It can be seen that the average  $\omega$  in Melpitz is obviously lower than those obtained in marine sites (Mace Head, WSA and BRW) in which the aerosol optical properties are dominated by sea salt. And the average  $\omega$  in Melpitz is similar as those measured in regional background site (BND, Hohenpeissenberg, K-Pusztá and SDZ) and the Mediterranean site (Finokalia) which influenced by anthropogenic and/or biomass burning activities.”*

*Table 8. Average  $\omega$  obtained in other long-term in-situ measurement around the world.*

$\omega$	$\lambda$ (nm)	Station and country	Type of station	period	instrumentation	reference
<b>0.871+-0.051</b> <b>0.891 @550 nm</b> <b>0.893 @530 nm</b> <b>0.894 @525 nm</b>	637	Melpitz, Germany			MAAP, Thermo; 3563 Nephelometer, TSI	This study
<b>0.88+-0.05</b>	525	SDZ, China	regional background	2003.9-2005.1	AE31 Aethalometer, Magee Scientific; M9003 Nephelometer, EcoTech	Yan et al., 2008
<b>0.92+-0.04</b>	530	K-Pusztá, Hungary	regional background	1998-1999	PSAP, Radiance Research; Nephelometer,	Molnár and Mészáros, 2001
<b>0.906+-0.067</b>	550	BND, U.S.	regional background	1996.9-2000.9	PSAP, Radiance Research; 3563 Nephelometer, TSI	Delene and Ogren, 2002
<b>0.932+-0.051</b>	550	SGP, U.S.	regional	1997.4-2000.9	PSAP, Radiance Research; 3563	Delene and

<b>0.953+-0.038</b>	550	WSA, U.S.	background marine	1994.11-2000.4	Nephelometer, TSI PSAP, Radiance Nephelometer, TSI	Research;	3563	Ogren, 2002 Delene and Ogren, 2002
<b>0.959+-0.040</b>	550	BRW, U.S.	marine	1997.10-2000.9	PSAP, Radiance Nephelometer, TSI	Research;	3563	Delene and Ogren, 2002
<b>0.89+-0.04</b>	550	Finokalia, Greece	marine	2001.3-2002.6	PSAP, Radiance Nephelometer, Radiance Research	Research;	M903	Vrekoussis et al., 2005
<b>0.941-0.997</b>	550	Mace Head, Ireland	marine	2000.1-2002.12	AES/AE9 3563/3551 Nephelometer, TSI	Aethalometer, Magee Scientific;		Jennings et al., 2003
<b>0.81 (0.74-0.86)</b>	525	Mukteshwar, India	mountain	2005.9-2007.9	AE31, Magee Nephelometer, EcoTech	Scientific;	M9003	Hyvärinen et al., 2009
<b>0.85-0.91</b>		Hohenpeissenberg, Germany	mountain	1999-2005	Aethalometer, Magee Thermo; 3563 Nephelometer, TSI	Scientific;	MAAP,	Kaminski, 2006
<b>0.84+-0.09</b>	637	Puijo, Finland	semiurban	2006.9-2010.9	MAAP, Thermo; 3563 Nephelometer, TSI			Leskinen et al., 2012
<b>0.86+-0.08</b>	637	Central Amazonia, Brazil	tropical forest	2008.2-2011.2	MAAP, Thermo; 3563 Nephelometer, TSI			Rizzo et al., 2013

### 11. Reviewer:

- p.27825: the wavelength difference between 2 measurement sites does not impede the comparison of the data. An absorption Angström exponent of -1 is usually applied to obtain the data at the right wavelength.

#### Response:

*Following the reviewer's suggestion, we assumed an absorption Angström exponent of -1, and corrected the  $\sigma_{ap}$  and  $\omega$  to other wavelengths in the comparison with the values in other long-term measurements.*

### 12. Reviewer:

- p. 27826, line 12: the single scattering albedo does not have a clear annual cycle!

#### Response:

*The sentence "It can be seen in Fig. 4 that annual cycles are evident for all the dry aerosol optical properties" in section 3.4 has been replaced with "It can be seen that annual variations can be found in all the dry aerosol optical properties. Some of them show evident annual cycles."*

### 13. Reviewer:

- p. 27826, lines 14-18: the high pollution events during winter are directly visible in Fig. 3 and not only in the statistics.

#### Response:

*Following the comment 10, figure 3 and the corresponding description has been already deleted.*

### 14. Reviewer:

- p. 27826: the single scattering albedo cycle seem to have higher values from March to June, which does completely correspond to "spring-summer"! Is the secondary aerosol production visible in SMPS measurements?

#### Response:

*Yes, the secondary aerosol production is evident in TDMPS measurement, as shown in the figure below of the average diurnal variation of aerosol number size distribution in the four seasons.*

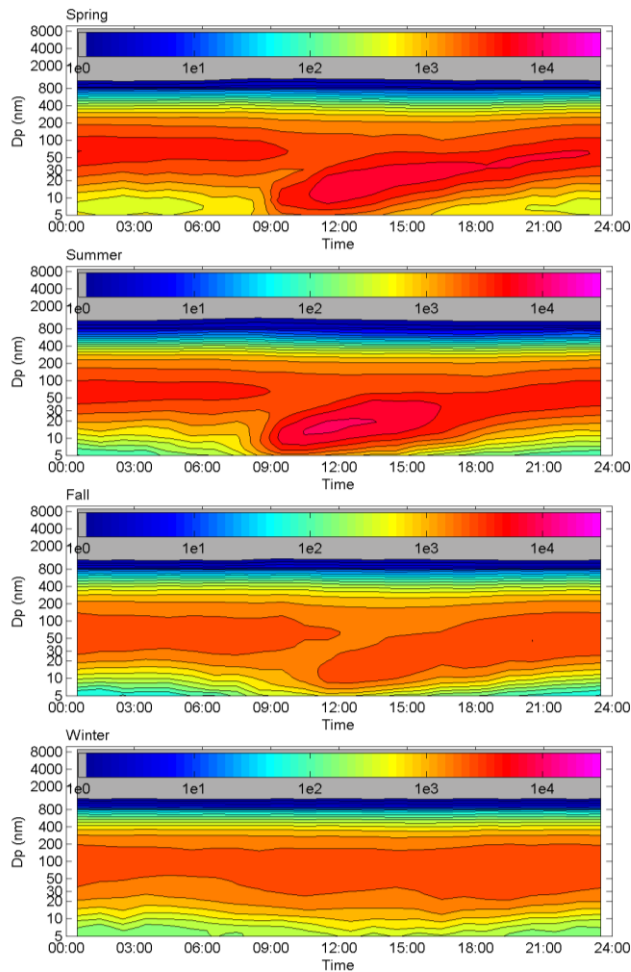


Figure 6. Average diurnal variation of aerosol number size distribution in the four seasons, based on the measurements of TDMPS and APS from 2008 to 2010.

It can be seen that, in spring and summer the new particle formation and the consequent growth of nucleation mode particles are evident. This figure has been added in the manuscript to help to explain the annual variation of single scattering albedo:

“Figure 6 shows the average diurnal variation of aerosol number size distribution in the four seasons, based on the measurements of TDMPS and APS from 2008 to 2010. It can be seen that new particle formation and the consequent growth of nucleation mode particles are evident in daytime in spring and summer. In these two seasons, secondary aerosol productions via photochemistry processes are efficient and results in a large fraction of non-light-absorbing components such as organic matter and sulfate in particulate matters (Poulain et al., 2011), hence yielding a relatively higher level of  $\omega$ . The “banana shape” can not be easily seen in fall and disappeared in winter, indicating the inhibition of secondary aerosol production in these two seasons, thus resulting in a relatively lower level of  $\omega$ .”

Figure 6 is also used for the explanation of the annual pattern of  $\alpha$  and  $b$ .

### 15. Reviewer:

- p. 27827: in winter, is there also a relation between the low single scattering albedo and greater contribution of carbon due to larger combustion processes (heating, fires, : : ) ?

**Response:**

*Yes, we believe that the emission from domestic heating is also an important reason for the dropping of  $\omega$  in winter. Therefore, we have added a sentence to clear this point:*

*“In winter, the local emission of black carbon is higher due to a larger amount of fossil fuel combustion. It was also found that the residential wood burning during the cold seasons has a significant contribution on the elemental carbon in Europe (Genberg et al., 2013). The higher emission of BC and less activity of aerosol aging and secondary aerosol formation causes a lower  $\omega$  in winter.”*

**16. Reviewer:**

-p. 27827: the discussion about the scattering Angström exponent should differentiate the cases calculated with the various wavelength pairs. The SMPS associated with Mie code could also explain the different annual cycles as a function of wavelength pairs.

**Response:**

*Following the reviewer’s suggestion, a figure and more discussions have been added in this section, as follows:*

*“One should also note that the  $\alpha$  for the two wavelength pairs show some difference in their annual patterns.  $\alpha_{450-550\text{nm}}$  in summer is at the similar level as  $\alpha_{550-700\text{nm}}$ , while in winter  $\alpha_{450-550\text{nm}}$  is lower than  $\alpha_{550-700\text{nm}}$ .  $\alpha_{450-550\text{nm}}$  therefore shows a more obvious annual variation compared with  $\alpha_{550-700\text{nm}}$ . This is because the  $\alpha$  for different wavelength pairs has different response on the variation of aerosol number size distribution. Figure 7 shows the measured  $\alpha_{450-550\text{nm}}$  and  $\alpha_{550-700\text{nm}}$  versus the corresponding effective radius of submicron aerosol. It can be found that  $\alpha_{450-550\text{nm}}$  is more sensitive to the variation of the effective radius of submicron aerosol than  $\alpha_{550-700\text{nm}}$ . With the increase of the effective radius of submicron aerosol,  $\alpha_{450-550\text{nm}}$  decrease with a steeper slope than  $\alpha_{550-700\text{nm}}$ . In the cases of  $r_{\text{eff}}$  lower than 120 nm (i.e. in summer), the two  $\alpha$  are in the similar level; while in the case of  $r_{\text{eff}}$  higher than 140 nm (i.e. in winter),  $\alpha_{450-550\text{nm}}$  is lower than  $\alpha_{550-700\text{nm}}$ .”*

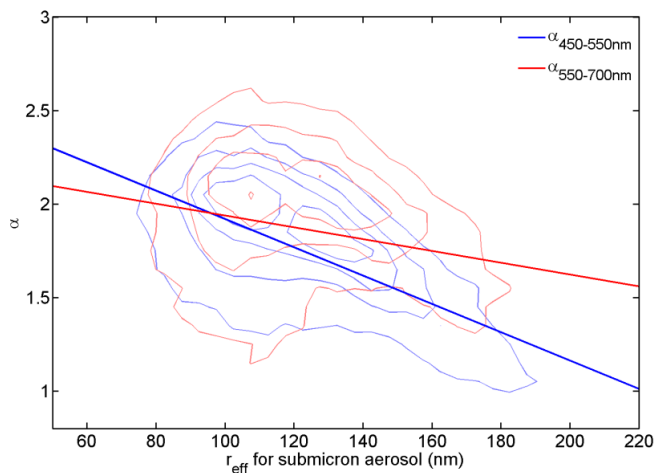


*Figure 7. Measured  $\alpha_{450-550\text{nm}}$  and  $\alpha_{550-700\text{nm}}$  versus the corresponding effective radius of submicron aerosol in the period of 2008-2010. To visualize the data distribution, the counts of data points are displayed as contour graphs. The red and blue straight lines represent the linear regression fits to the data.*

**17. Reviewer:**

-§3.5: the discussion about the influence of the different air masses is not straightforward and to some extent has the same conclusion than the annual cycle: in winter there is higher concentration due to the

lower mixing layer high than in summer. P.27830: a figure could explain explicitly that “the fine mode effective radius seems to be more important than the fine mode volume fraction in explaining the variation of the Angström exponent? the same correlation could be done with b.

**Response:**

*Thanks for this comments. We have revised the relating paragraphs and figures to make it easier to read. And fig. 6 and 7 were merged together and modified as fig. 9. The histograms are sorted according to a descending scattering coefficient  $\sigma_{sp}$  at 550 nm. As shown below:*

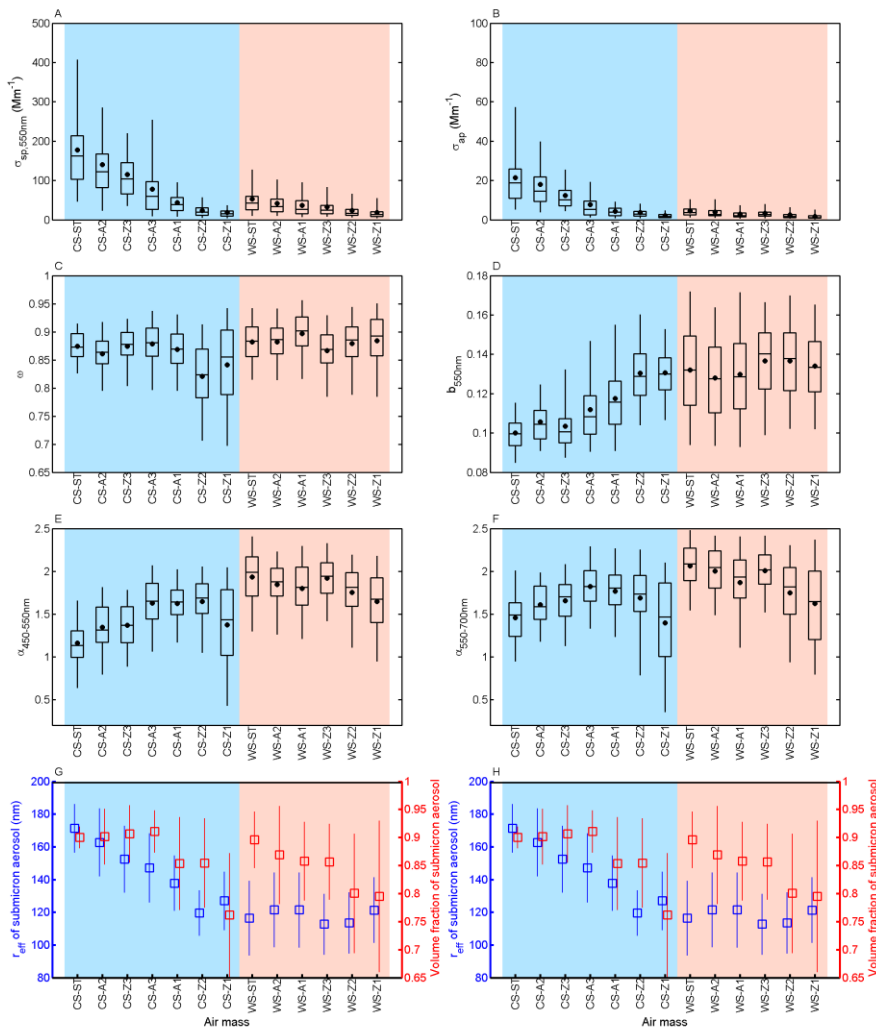


*Figure 9. Average aerosol scattering coefficient (A), absorption coefficient (B), single scattering albedo (C), hemispheric backscattering fraction (D), Ångström exponent at 450-550 nm (E) and at 550-700 nm (F) for the 13 air mass types. For each panel, the boxes and whiskers denote the 5, 25, 50, 75 and 95 percentiles, while the dots denote the mean values. To have a clear comparison, average effective radius (blue) and volume fraction (red) of submicron aerosol for the 13 air mass types is also shown in (G) and (H), in which whiskers denote the standard deviation.*

*To better explain that “the fine mode effective radius seems to be more important than the fine mode volume fraction in explaining the variation of the Angström exponent”, a figure has been added. And the relating discussion has been revised, as shown below:*

“It can be noted that due to the favorable condition for pollutant accumulation during the cold season, both of the two parameters are very sensitive to the originating area and the air mass residence time in the continental atmosphere, and an inverse relationship can be found between the  $\alpha$  and the fine mode effective radius. In the warm season, however, the fine mode aerosol effective radii are similar for all air mass types, and lower than in cold season. Also the  $\alpha$  for all air mass types in warm season is similar, and higher than those in cold season. The fine mode effective radius therefore seems to be more important than the fine mode volume fraction in explaining the variation of  $\alpha$ . To prove this presumption, fig. 10 shows the correlation between  $\alpha$  and the corresponding volume fraction and effective radius of fine mode aerosol. A clear inverse correlation can be found between  $\alpha$  and the effective radius of fine mode aerosol. However, only weak positive correlations can be found between  $\alpha$  and the volume fraction of fine mode aerosol for some ranges of volume fraction. This means that for the natural variation of aerosol number size distribution in Central Europe, both fine mode effective radius and volume fraction are important in explaining the variation of  $\alpha$ , but the fine mode effective radius is more crucial.”  
The same correlations for  $b$  were also included in fig. 10.

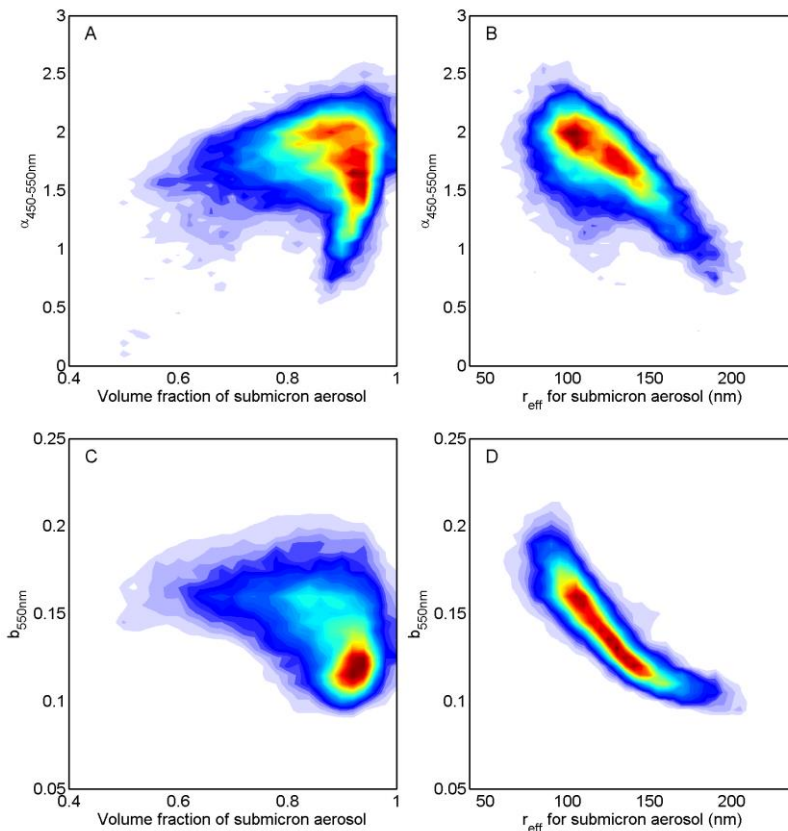


Figure 10. Correlation between  $\alpha$  and volume fraction of submicron aerosol(A),  $\alpha$  and effective radius of submicron aerosol (B),  $b$  and volume fraction of submicron aerosol (C),  $b$  and effective radius of submicron aerosol (D). To visualize the data distribution, the counts of data points are displayed as an intensity graph.

### 18. Reviewer:

- p. 27830 last §: the first 2 sentence compare the  $b$  as a function of season. The third one gives a reference comparing  $b$  and the particle size. Could you please better explain where the inversion in the relationship is? The Mie code could also reproduce all these relationships?

**Response:**

To better explain the relationship between  $b$  and particle size, and between  $b$  and aerosol mixing state, the single particle hemispheric backscattering fraction was calculated based on Mie model. The result is shown in fig. Z. And the paragraph has been rewritten, as shown below:

“From fig. 9(D) and (H), an evident inverse correlation can be found between  $b$  and the effective radius of submicron aerosol for all the 13 air mass types, implying that the variation of  $b$  is mainly induced by the variation of the shape of particle number size distribution. This results are in accord with Collaud Coen et al. (2007). Ma et al. (2012) found that  $b$  is also determined by the mixing state of light absorbing carbon. To better study the dependence of  $b$  on these two parameters, the single particle hemispheric backscattering fraction was calculated based on Mie model. In the calculation, two mixing states were assumed: BC externally mixed and BC coated with light-scattering material. The volume fraction of BC was set as 0.058, the average value during the whole period. More details of the calculation refer to section 2.2. Results are shown in fig. 11.  $b$  shows a high dependence on the particle size. Especially in the range of 100 to 300 nm,  $b$  drops down steeply with the increase of particle size. After 300 nm,  $b$  fluctuates with increase size. This result can basically explain the inverse relationship between  $b$  and the effective radius of submicron aerosol. One should note that the mixing state of black carbon also influences  $b$ .  $b$  calculated based on core-shell mixture is clearly higher than that calculated based on external mixture. However, the influence of mixing state is less than that of the particle size. It can be seen in fig. 10(D) that  $b$  is highly correlated with the effective radius of submicron aerosol. The air mass distribution of  $b$  exhibits different characteristics in cold and warm season. In warm season, due to the frequent occurrence of new particle formation events,  $b$  for most of the air mass types are higher than those in cold season. The  $b$  in warm season also shows a wider probability distribution than in cold season. It can be seen in fig. 11 that the dependence of  $b$  on particle size gets higher with the decrease of particle size. Therefore, with lower effective radii in summer, the  $b$  show a higher variability.”

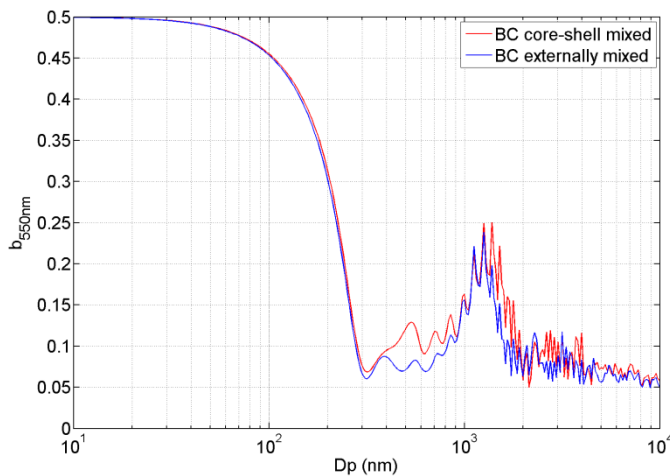


Figure 11. Single particle hemispheric backscattering fraction calculated based on Mie model, assuming core-shell mixture (red line) and external mixture (blue line) of black carbon and light-scattering material.

**19. Reviewer:**

- p. 27830 last §: a figure could present the inverse correlation between  $b$  and the effective radius of submicron particles?

**Response:**

A new figure has been added in the manuscript (fig. 11), as shown in the response of comment 18.

## 20. Reviewer:

-Table 2 reports  $\log(b)$  and not  $b$  according to the text p. 27820

## Response:

*The values listed in table 2 is actually the parameter  $b$  in the fitting formula  $\log(\sigma_{\text{calculated}}) = \log(b) + \log(\sigma_{\text{measured}})$ , not  $\log(b)$ . To make it more clear, the title of table 2 has been revised as:*

*“Table 2. The fitting parameters ( $b$  and  $R^2$ ) of the linear fittings for calculated and measured  $\sigma_{\text{sp}}$  and  $\sigma_{\text{bsp}}$  with  $\log(\sigma_{\text{calculated}}) = \log(b) + \log(\sigma_{\text{measured}})$ .”*

## 21. Reviewer:

- Fig. 4: the annual cycle of  $N$ =sum of all SMPS could be also presented?

## Response:

*Thanks for this suggestion. We have added the annual cycle of aerosol total number concentration and the effective radius of submicron aerosol in the figure, as shown below. They have been also included in the discussion of the annual variation of aerosol optical properties.*

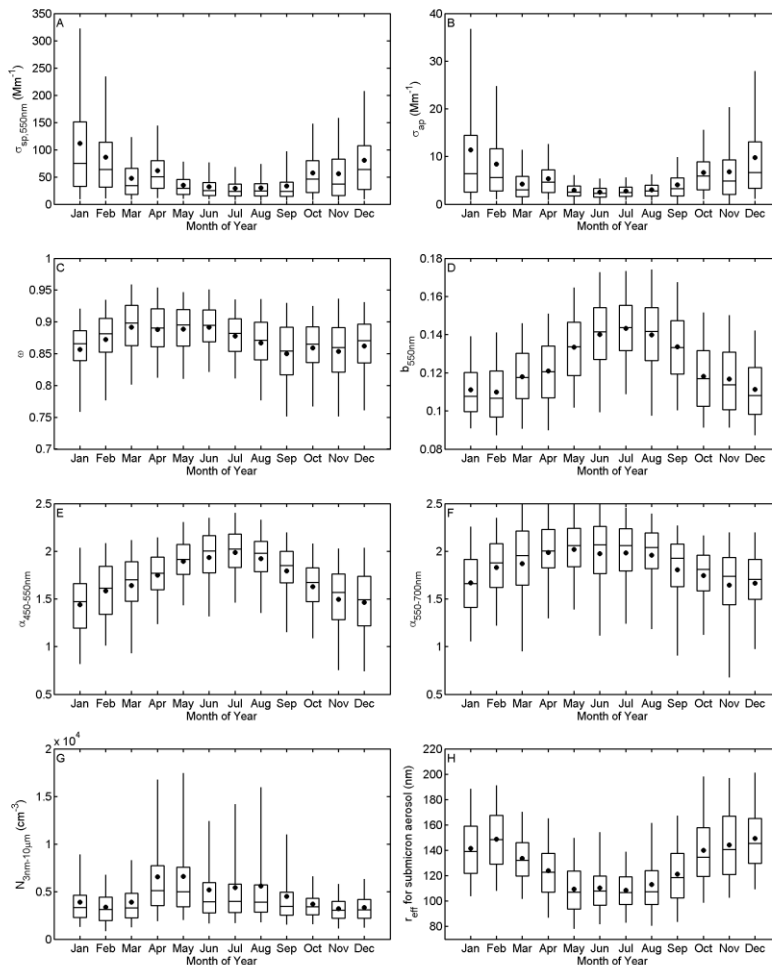


*Figure 5. Annual variations of aerosol scattering coefficient (A), absorption coefficient (B), single scattering albedo (C), hemispheric backscattering fraction (D), Ångström exponent at 450-550 nm (E) and*

at 550-700 nm (F), aerosol total number concentration (G), and the effective radius of submicron aerosol. For each panel, the boxes and whiskers denote the 5, 25, 50, 75 and 95 percentiles, while the dots denote the mean values.

## 22. Reviewer:

- Fig. 5 should be given with §2.3

### Response:

*This figure has been given in section 2.3 as figure 1.*

## 23. Reviewer:

- fig. 6: air masses cannot be easily read.

### Response:

*The figure has been revised, as shown in the reply of comment 17.*

## Reference

- Anderson, T. L., Covert, D. S., Marshall, S. F., Laucks, M. L., Charlson, R. J., Waggoner, A. P., Ogren, J. A., Caldwell, R., Holm, R. L., Quant, G., Sem, J., Wiedensohler, A., Ahlquist, N. A., Bates, T. S.: Performance characteristics of a High-sensitivity, three-wavelength total scatter/backscatter nephelometer, *Journal of Atmospheric and Oceanic Technology*, 13, 967 – 986, 1996.
- Anderson, T. L., and Ogren, J. A.: Determining aerosol radiative properties using the TSI 3563 Integrating Nephelometer. *Aerosol Sci. Technol.*, 29, 57 – 69, 1998.
- Asmi, A., Wiedensohler, A., Laj, P., Fjaeraa, A.-M., Sellegri, K., Birmili, W., Weingartner, E., Baltensperger, U., Zdimal, V., Zikova, N., Putaud, J.-P., Marinoni, A., Tunved, P., Hansson, H.-C., Fiebig, M., Kivekäs, N., Lihavainen, H., Asmi, E., Ulevicius, V., Aalto, P. P., Swietlicki, E., Kristensson, A., Mihalopoulos, N., Kalivitis, N., Kalapov, I., Kiss, G., de Leeuw, G., Henzing, B., Harrison, R. M., Beddows, D., O'Dowd, C., Jennings, S. G., Flentje, H., Weinhold, K., Meinhardt, F., Ries, L., and Kulmala, M.: Number size distributions and seasonality of submicron particles in Europe 2008–2009, *Atmos. Chem. Phys.*, 11, 5505-5538, 2011.
- Birmili, W., K. Weinhold, S. Nordmann, A. Wiedensohler, G. Spindler, K. Müller, H. Herrmann, T. Gnauk, M. Pitz, J. Cyrus, H. Flentje, C. Nickel, T.A.J. Kuhlbusch, G. Löschau, D. Haase, F. Meinhardt, A. Schwerin, L. Ries, and K. Wirtz. Atmospheric aerosol measurements in the German Ultrafine Aerosol Network (GUAN): Part 1 - soot and particle number size distributions. *Gefahrst. Reinh. Luft*, 69(4): 137-145, 2009.
- Birmili, W., Heinke, K., Pitz, M., Matschullat, J., Wiedensohler, A., Cyrus, J., Wichmann, H.-E., and Peters, A.: Particle number size distributions in urban air before and after volatilisation, *Atmos. Chem. Phys.*, 10, 4643-4660, doi: 10.5194/acp-10-4643-2010, 2010.
- Bohren, C. F., and Huffman, D. R.: *Absorption and Scattering of Light by Small Particles*, John Wiley, Hoboken, N. J., 1983.
- Cheng, Y. F., Berghof, M., Garland, R. M., Wiedensohler, A., Wehner, B., Müller, T., Su, H., Zhang, Y. H., Achtert, P., Nowak, A., Pöschl, U., Zhu, T., Hu, M., Zeng, L. M.: Influence of soot mixing state on aerosol light absorption and single scattering albedo during air mass aging at a polluted regional site in northeastern China, *J. Geophys. Res.*, 114, D00G10, doi: 10.1029/2008JD010883, 2009.

- Collaud Coen, M., Weingartner, E., Nyeki, S., Cozic, J., Henning, S., Verheggen, B., Gehrig, R., Baltensperger, U.: Long-term trend analysis of aerosol variables at the high-alpine site Jungfraujoch, *J. Geophys. Res.*, 112, D13213, doi:10.1029/2006JD007995, 2007.
- Delene, D. J. and Ogren, J. A.: Variability of Aerosol Optical Properties at Four North American Surface Monitoring Sites, *J. Atmos. Sci.*, 59, 1135 – 1150, 2002.
- Dittmann, E., Barth, S., Lang, J., Müller-Westermeier, G.: Objektive Wetterlagenklassifikation (Objective weather type classification), Ber. Dt. Wetterd. 197, Offenbach a. M., Germany (in German), 1995.
- Draxler, R. R. and Hess, G. D.: Description of the Hysplit\_4 Modeling System, NOAA, Technical Memorandum ERL ARL-224, 25 pp, 2004.
- Engler, C., D. Rose, B. Wehner, A. Wiedensohler, E. Brüggemann, T. Gnauk, G. Spindler, T. Tuch, W. Birmili. Size distributions of non-volatile particle residuals ( $D_p < 800$  nm) at a rural site in Germany and relation to air mass origin. *Atmos. Chem. Phys.* 7: 5785-5802, 2007.
- Genberg, J., Denier van der Gon, H. A. C., Simpson, D., Swietlicki, E., Areskou, H., Beddows, D., Ceburnis, D., Fiebig, M., Hansson, H. C., Harrison, R. M., Jennings, S. G., Saarikoski, S., Spindler, G., Visschedijk, A. J. H., Wiedensohler, A., Yttri, K. E., and Bergström, R.: Light-absorbing carbon in Europe – measurement and modelling, with a focus on residential wood combustion emissions, *Atmos. Chem. Phys.*, 13, 8719-8738, doi:10.5194/acp-13-8719-2013, 2013.
- Heintzenberg, J., Birmili, W., Otto, R., Andreae, M. O., Mayer, J.-C., Chi, X., and Panov, A.: Aerosol particle number size distributions and particulate light absorption at the ZOTTO tall tower (Siberia), 2006–2009, *Atmos. Chem. Phys.*, 11, 8703-8719, doi:10.5194/acp-11-8703-2011, 2011.
- Hess P., Brezowsky, H.: Katalog der Großwetterlagen Europas (Catalog of the European Large Scale Weather Types). Ber. Dt. Wetterd. in der US-Zone 33, Bad Kissingen, Germany (in German), 1952.
- Hyvärinen, A. P., Lihavainen, H., Komppula, M., Sharma, V. P., Kerminen, V. M., Panwar, T. S., Viisanen, Y.: Continuous measurements of optical properties of atmospheric aerosols in Mukteshwar, northern India, *J. Geophys. Res.*, 114, D08207, doi:10.1029/2008JD011489, 2009
- Jennings, S. G., Kleefeld, C., O'Dowd, C. D., Junker, C., Spain, T. G., O'Brien, P., Roddy, A. F., O'Connor, T. C.: Mace Head Atmospheric Research Station-characterization of aerosol radiative parameters, *Boreal environment research*, 8(4), 303-314, 2003
- Kaminski, U.: Aktuelle Aerosoltrends an der GAW Globalstation Hohenpeißenberg und ihre Relevanz für Luftreinhaltung und Klima, *Umweltwissenschaften und Schadstoff-Forschung*, 18(2), 88-94, 2006
- Leskinen, A., Arola, A., Komppula, M., Portin, H., Tiitta, P., Miettinen, P., Romakkaniemi, S., Laaksonen, A., Lehtinen, K. E. J.: Seasonal cycle and source analyses of aerosol optical properties in a semi-urban environment at Puijo station in Eastern Finland, *Atmos. Chem. Phys.*, 12, 5647–5659, 2012
- Ma, N., Zhao, C. S., Nowak, A., Müller, T., Pfeifer, S., Cheng, Y. F., Deng, Z.Z., Liu, P. F., Xu, W. Y., Ran, L., Yan, P., Göbel, T., Hallbauer, E., Mildnerberger, K., Henning, S., Yu, J., Chen, L. L., Zhou, X. J., Stratmann, F., and Wiedensohler, A.: Aerosol optical properties in the North China Plain during HaChi campaign: an in-situ optical closure study, *Atmos. Chem. Phys.*, 11, 5959-5973, doi:10.5194/acp-11-5959-2011, 2011.
- Ma, N., Zhao, C. S., Müller, T., Cheng, Y. F., Liu, P. F., Deng, Z. Z., Xu, W. Y., Ran, L., Nekat, B., van Pinxteren, D., Gnauk, T., Müller, K., Herrmann, H., Yan, P., Zhou, X. J., and Wiedensohler, A.: A new method to determine the mixing state of light absorbing carbonaceous using the measured aerosol optical properties and number size distributions, *Atmos. Chem. Phys.*, 12, 2381-2397, doi:10.5194/acp-12-2381-2012, 2012
- Mie, G.: Beiträge zur optic trüber Medien speziell kolloidaler Metallösungen, *Ann. Phys.*, 25, 377–445, 1908

- Molnár, A. and Mészáros, E.: On the relation between the size and chemical composition of aerosol particles and their optical properties, *Atmos. Environ.*, 35(30), 5053-5058, 2001.
- IPCC 2013: Myhre, G., D. Shindell, F.-M. Bréon, W. Collins, J. Fuglestedt, J. Huang, D. Koch, J.-F. Lamarque, D. Lee, B. Mendoza, T. Nakajima, A. Robock, G. Stephens, T. Takemura and H. Zhang, 2013: Anthropogenic and Natural Radiative Forcing. In: *Climate Change 2013: The Physical Science Basis. Contribution of Working Group I to the Fifth Assessment Report of the Intergovernmental Panel on Climate Change* [Stocker, T.F., D. Qin, G.-K. Plattner, M. Tignor, S.K. Allen, J. Boschung, A. Nauels, Y. Xia, V. Bex and P.M. Midgley (eds.)]. Cambridge University Press, Cambridge, United Kingdom and New York, NY, USA.
- Petzold, A., and Schönlinner, M.: Multi-angle absorption photometry a new method for the measurement of aerosol light absorption and atmospheric black carbon, *J. Aerosol Sci.*, 35, 421 – 441, 2004.
- Philipp, A., Bartholy, J., Beck, C., Erpicum, M., Esteban, P., Fettweis, X. et al.: Cost733cat—A database of weather and circulation type classifications. *Physics and Chemistry of the Earth, Parts A/B/C*, 35(9), 360-373, 2010.
- Poulain, L., Spindler, G., Birmili, W., Plass-Dülmer, C., Wiedensohler, A., Herrmann, H.: Seasonal and diurnal variations of particulate nitrate and organic matter at the IFT research station Melpitz, *Atmos. Phys. Chem.*, 11, 12579-12599, 2011.
- Rizzo, L. V., Artaxo, P., Müller, T., Wiedensohler, A., Paixão, M., Cirino, G. G., Arana, A., Swietlicki, E., Roldin, P., Fors, E. O., Wiedemann, K. T., Leal, L. S. M., Kulmala, M.: Long term measurements of aerosol optical properties at a primary forest site in Amazonia, *Atmos. Chem. Phys.*, 13, 2391–2413, 2013
- Vrekoussis, M., Liakakou, E., Kocak, M., Kubilay, N., Oikonomou, K., Sciare, J., & Mihalopoulos, N.: Seasonal variability of optical properties of aerosols in the Eastern Mediterranean, *Atmos. Environ.*, 39(37), 7083-7094, 2005.
- Wex, H., Neusüß C., Wendisch M., Stratmann F., Koziar C., Keil A., Wiedensohler A., Ebert M.: Particle scattering, backscattering, and absorption coefficients: An in situ closure and sensitivity study, *J. Geophys. Res.*, 107(D21), 8122, doi: 10.1029/2000JD000234, 2002
- Wiedensohler, A., Birmili, W., Nowak, A., Sonntag, A., Weinhold, K., Merkel, M., Wehner, B., Tuch, T., Pfeifer, S., Fiebig, M., Fjåraa, A. M., Asmi, E., Sellegri, K., Depuy, R., Venzac, H., Villani, P., Laj, P., Aalto, P., Ogren, J. A., Swietlicki, E., Williams, P., Roldin, P., Quincey, P., Hüglin, C., Fierz-Schmidhauser, R., Gysel, M., Weingartner, E., Riccobono, F., Santos, S., Gruning, C., Faloon, K., Beddows, D., Harrison, R., Monahan, C., Jennings, S. G., O'Dowd, C. D., Marinoni, A., Horn, H.-G., Keck, L., Jiang, J., Scheckman, J., McMurry, P. H., Deng, Z., Zhao, C. S., Moerman, M., Henzing, B., de Leeuw, G., Löschau, G., and Bastian, S.: Mobility particle size spectrometers: harmonization of technical standards and data structure to facilitate high quality long-term observations of atmospheric particle number size distributions, *Atmos. Meas. Tech.*, 5, 657-685, 2012.
- Yan, P., Tang, J., Huang, J., Mao, J. T., Zhou, X. J., Liu, Q., Wang, Z. F., Zhou, H. G.: The measurement of aerosol optical properties at a rural site in Northern China, *Atmos. Chem. Phys.*, 8, 2229 – 2242, 2008.

## Appendix – list of the figures in the revised manuscript

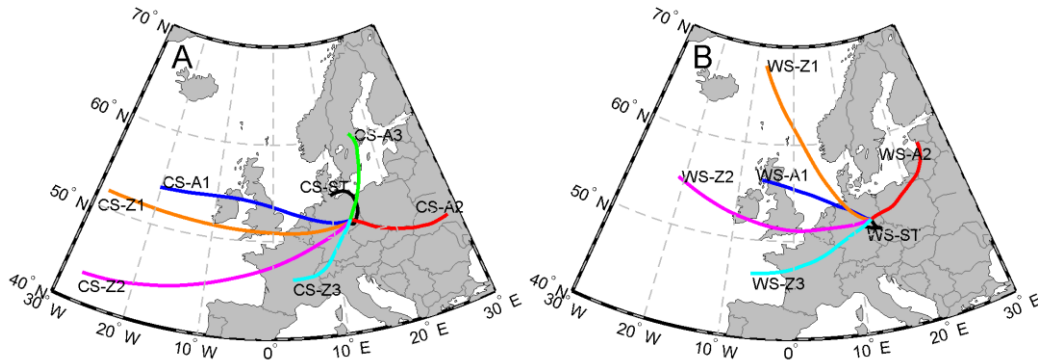


Figure 1. Average back trajectories, terminating at Melpitz, for the 13 air mass types investigated. (A) and (B) display the air mass types associated with more stable stratification (CS - cold season) and less stable stratification (WS – warm season), respectively. The duration of the backtrajectories is 72 h.

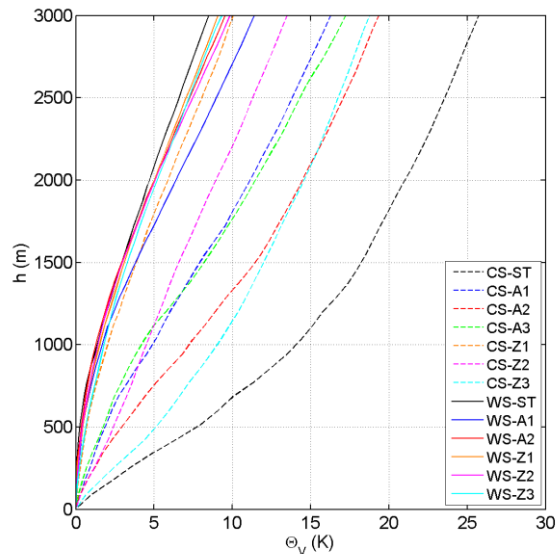


Figure 2. Average normalized profiles of pseudopotential temperature ( $\vartheta_v$ ) for the 13 air mass types reported. Profiles with a flat gradient indicate a temperature inversion. Profiles with a steep gradient imply stratification close to neutral. Data originate from the radiosoundings launched at the DWD station Lindenberg, located 115 km northeast of Melpitz.

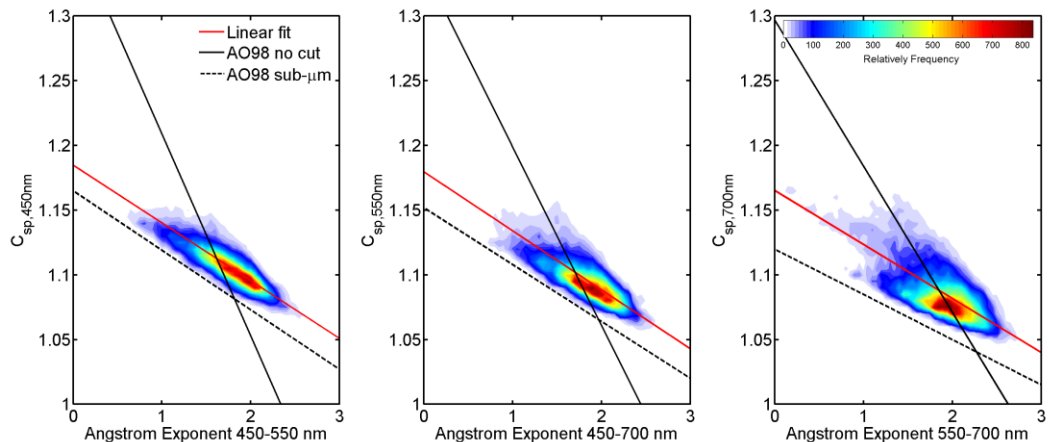


Figure 3. Correlation between calculated  $C_{sp}$  and measured  $\alpha$  for the three operating wavelengths for TSI 3563 nephelometer. The red straight lines represent the linear regression fits to the data. To visualize the data distribution, the counts of data points are displayed as an intensity graph.

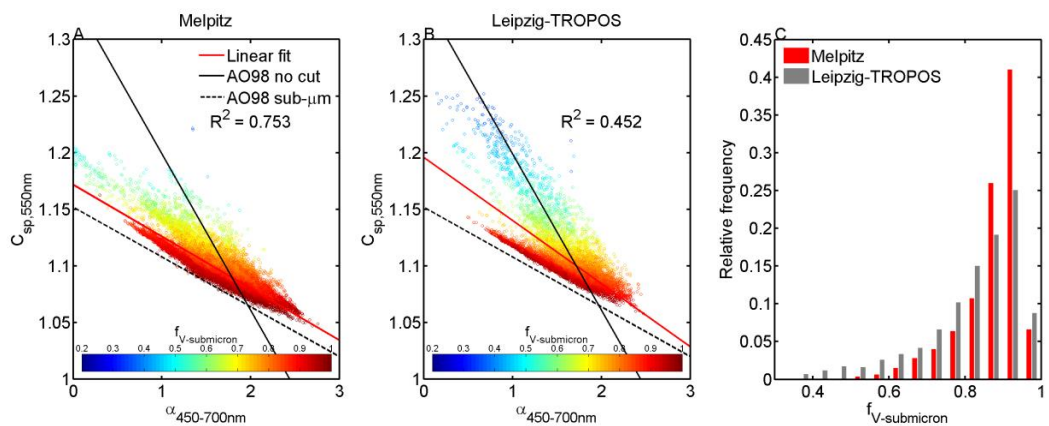


Figure 4. Correlation between calculated  $C_{sp}$  and measured  $\alpha_{450-700\text{nm}}$  at Melpitz (A) and Leipzig-TROPOS (B). Colors of dots denote the corresponding volume fraction of submicron aerosol to total aerosol. The red straight lines represent the linear regression fits to the data. (C) The relative frequency distribution of the volume fraction of submicron aerosol in Melpitz and Leipzig-TROPOS.

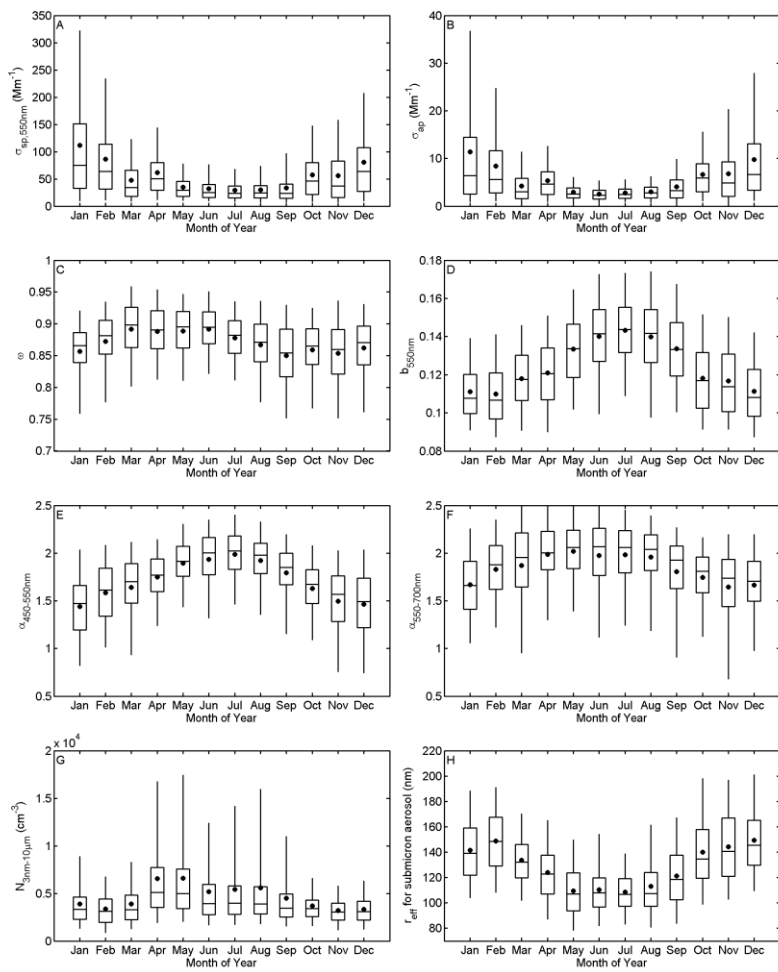


Figure 5. Annual variations of aerosol scattering coefficient (A), absorption coefficient (B), single scattering albedo (C), hemispheric backscattering fraction (D), Ångström exponent at 450-550 nm (E) and at 550-700 nm (F), aerosol total number concentration (G), and the effective radius of submicron aerosol. For each panel, the boxes and whiskers denote the 5, 25, 50, 75 and 95 percentiles, while the dots denote the mean values.

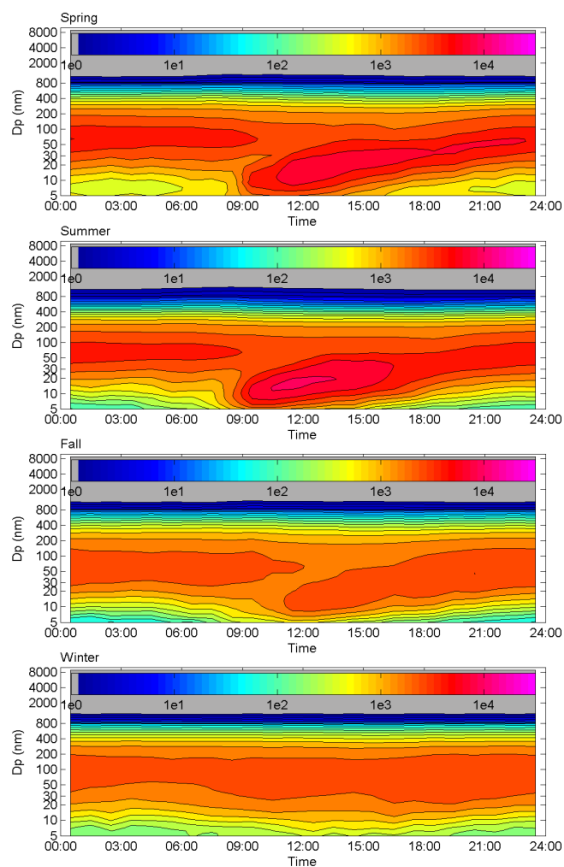


Figure 6. Average diurnal variation of aerosol number size distribution in the four seasons, based on the measurements of TDMPS and APS from 2008 to 2010.

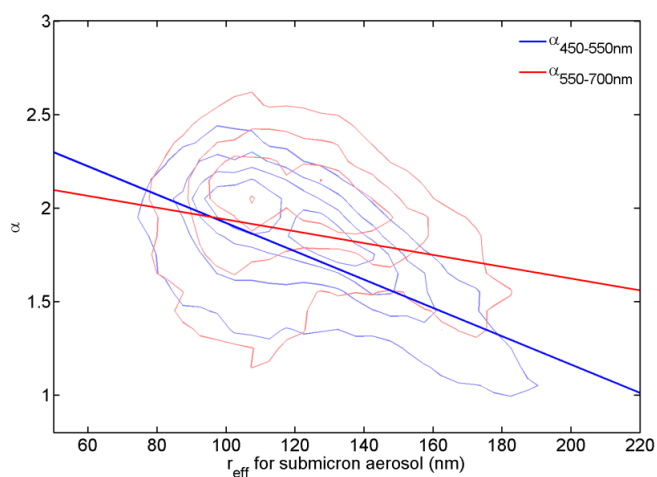


Figure 7. Measured  $\alpha_{450-550nm}$  and  $\alpha_{550-700nm}$  versus the corresponding effective radius of submicron aerosol in the period of 2008-2010. To visualize the data distribution, the counts of data points are displayed as contour graphs. The red and blue straight lines represent the linear regression fits to the data.

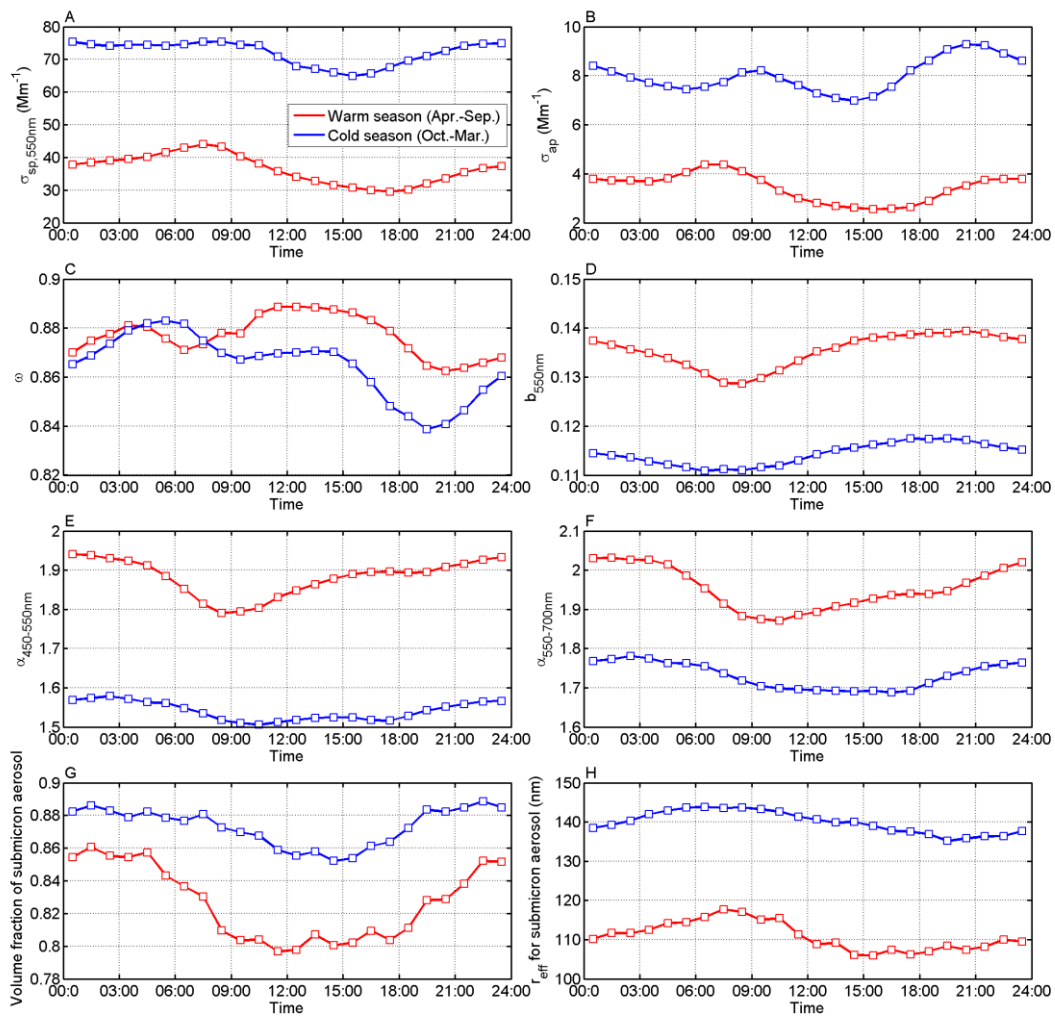


Figure 8. Average diurnal variations of aerosol scattering coefficient (A), absorption coefficient (B), single scattering albedo (C), hemispheric backscattering fraction (D), Ångström exponent at 450-550 nm (E) and at 550-700 nm (F), volume fraction of submicron aerosol (G), and the effective radius of submicron aerosol. For each panel, the red and blue lines represent the results of warm (Apr.-Sep.) and cold season (Oct.-Mar.), respectively.

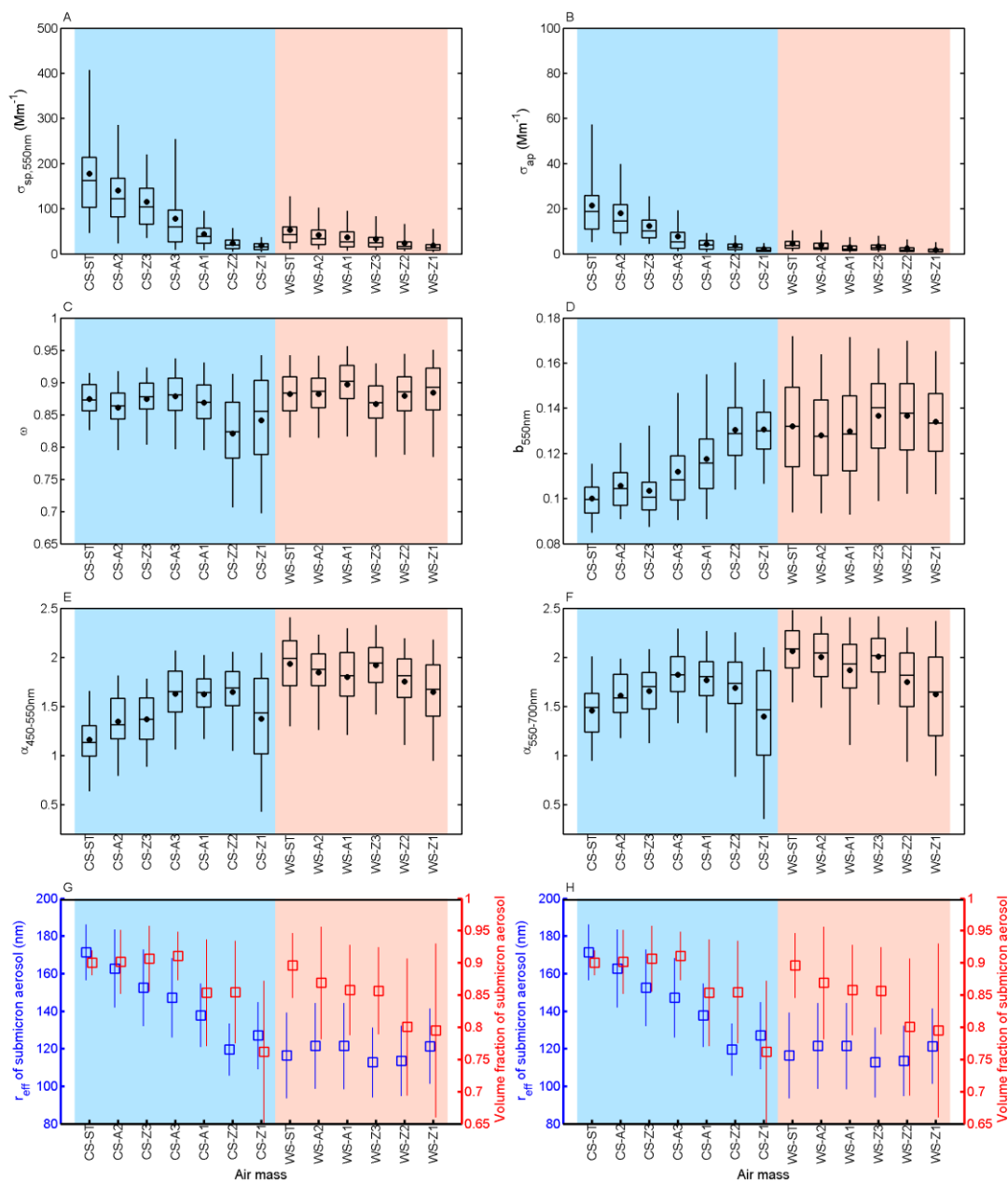


Figure 9. Average aerosol scattering coefficient (A), absorption coefficient (B), single scattering albedo (C), hemispheric backscattering fraction (D), Ångström exponent at 450-550 nm (E) and at 550-700 nm (F) for the 13 air mass types. For each panel, the boxes and whiskers denote the 5, 25, 50, 75 and 95 percentiles, while the dots denote the mean values. To have a clear comparison, average effective radius (blue) and volume fraction (red) of submicron aerosol for the 13 air mass types is also shown in (G) and (H), in which whiskers denote the standard deviation.

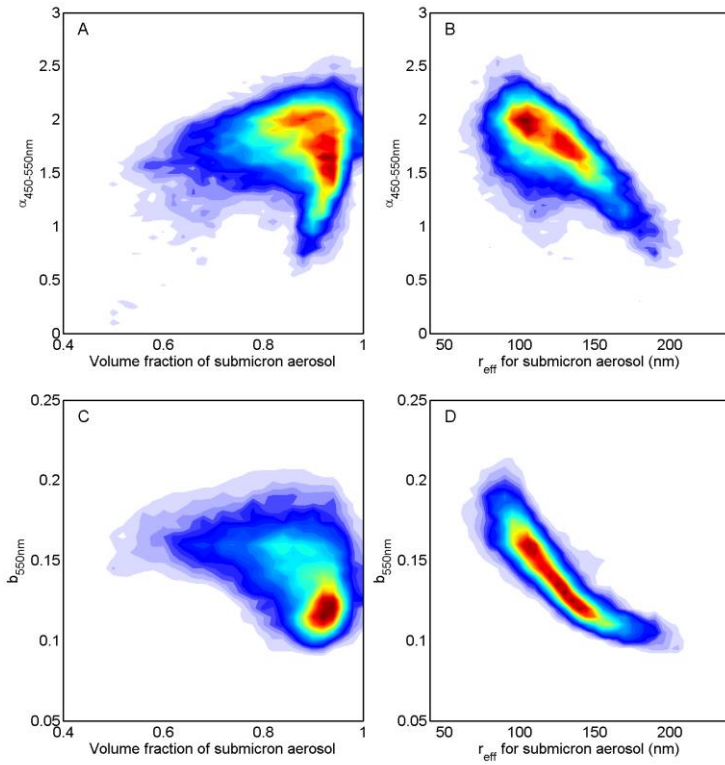


Figure 10. Correlation between  $\alpha$  and volume fraction of submicron aerosol(A),  $\alpha$  and effective radius of submicron aerosol (B),  $b$  and volume fraction of submicron aerosol (C),  $b$  and effective radius of submicron aerosol (D). To visualize the data distribution, the counts of data points are displayed as an intensity graph.

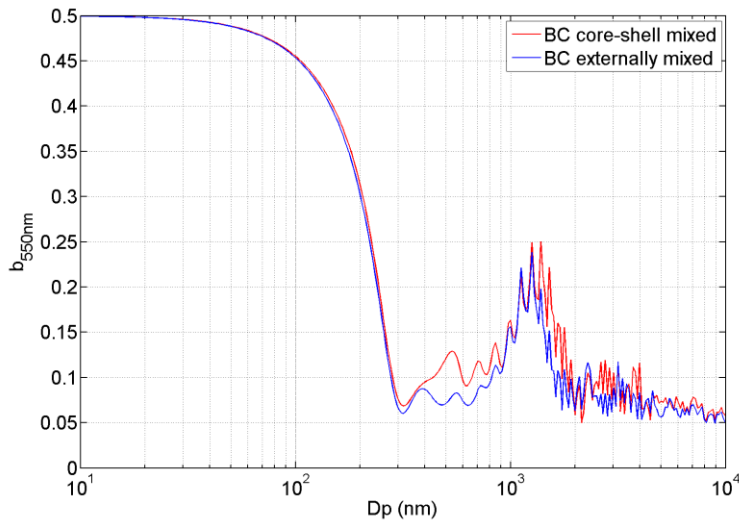


Figure 11. Single particle hemispheric backscattering fraction calculated based on Mie model, assuming core-shell mixture (red line) and external mixture (blue line) of black carbon and light-scattering material.

## **Supplementary material**

The second and third air mass classification scheme are established schemes that took part in comparisons of the Cost 733 action (Philipp et al., 2010).

The Hess and Brezowsky Grosswetterlagen scheme (Cost No. 1, “HBGWL”) is a subjective method in which days are classified according to the shape of atmospheric pressure fields, with a focus on the 500 hPa geopotential surface (Hess and Brezowsky, 1952). HBGWL distinguishes three orientations of atmospheric flow over Central Europe: zonal, meridional, and mixed. According to the type of flow (cyclonic or anticyclonic) and the location of its controlling centres of high and low pressure, a total of 29 weather types are distinguished (Gerstengarbe and Werner, 2005). Daily classification data for the HBGWL scheme were retrieved for the period 2007-2011 from the German Weather Service website ([www.dwd.de](http://www.dwd.de)). The nomenclature of the Hess and Brezowsky Grosswetterlagen can be seen in Table S1, as copied from James et al. (2007).

Objective Weather Classification (Cost No. 19, “WLKC09”) is an objective weather classification scheme for Central Europe that distinguishes days according to the type of flow (cyclonic/ anticyclonic) on the 1000 hPa and the 700 hPa geopotential levels, according to the predominant wind direction on the 700 hPa geopotential level, and on the degree of moisture in the atmosphere (Dittmann, 1995). The combination of these criteria leads to a distinction of a total of 40 weather types. Daily classification data for the WLKC09 scheme were also retrieved for the period 2007-2011 from the German Weather Service website ([www.dwd.de](http://www.dwd.de)). A description of the nomenclature is given on the next page.

**Table 1.** The 29 Grosswetterlagen with original German and translated English definitions

GWL	Original definition (German)	Translated definition (English)
01 WA	Westlage, antizyklonal	Anticyclonic Westerly
02 WZ	Westlage, zyklonal	Cyclonic Westerly
03 WS	Südliche Westlage	South-Shifted Westerly
04 WW	Winkelförmige Westlage	Maritime Westerly (Block E. Europe)
05 SWA	Südwestlage, antizyklonal	Anticyclonic South-Westerly
06 SWZ	Südwestlage, zyklonal	Cyclonic South-Westerly
07 NWA	Nordwestlage, antizyklonal	Anticyclonic North-Westerly
08 NWZ	Nordwestlage, zyklonal	Cyclonic North-Westerly
09 HM	Hoch Mitteleuropa	High over Central Europe
10 BM	Hochdruckbrücke (Rücken) Mitteleuropa	Zonal Ridge across Central Europe
11 TM	Tief Mitteleuropa	Low (Cut-Off) over Central Europe
12 NA	Nordlage, antizyklonal	Anticyclonic Northerly
13 NZ	Nordlage, zyklonal	Cyclonic Northerly
14 HNA	Hoch Nordmeer-Inland, antizyklonal	Icelandic High, Ridge C. Europe
15 HNZ	Hoch Nordmeer-Inland, zyklonal	Icelandic High, Trough C. Europe
16 HB	Hoch Britische Inseln	High over the British Isles
17 TRM	Trog Mitteleuropa	Trough over Central Europe
18 NEA	Nordostlage, antizyklonal	Anticyclonic North-Easterly
19 NEZ	Nordostlage, zyklonal	Cyclonic North-Easterly
20 HFA	Hoch Fennoskandien, antizyklonal	Scandinavian High, Ridge C. Europe
21 HFZ	Hoch Fennoskandien, zyklonal	Scandinavian High, Trough C. Europe
22 HNFA	Hoch Nordmeer-Fennoskandien, antizykl.	High Scandinavia-Iceland, Ridge C. Europe
23 HNFZ	Hoch Nordmeer-Fennoskandien, zyklonal	High Scandinavia-Iceland, Trough C. Europe
24 SEA	Südostlage, antizyklonal	Anticyclonic South-Easterly
25 SEZ	Südostlage, zyklonal	Cyclonic South-Easterly
26 SA	Südlage, antizyklonal	Anticyclonic Southerly
27 SZ	Südlage, zyklonal	Cyclonic Southerly
28 TB	Tief Britische Inseln	Low over the British Isles
29 TRW	Trog Westeuropa	Trough over Western Europe

Table S1: Nomenclature of the Hess and Brezowsky Grosswetterlagen (HBGWL), copied from James et al. (2007).

The nomenclature of the WLKC09 (Dittmann, 1995) is illustrated for the case of “NWAZT” as follows: “NW” = dominating wind direction (northwest) in Central Europe on the 700 hPa geopotential level. Other options: SW (southwest), SO (southeast), NO (northeast), X (undefined, in case no more than 2/3 of the wind vectors belong to a single sector).

“A” = anticyclonic flow in Central Europe on the 1000 hPa geopotential level, i.e. near the surface. Other option is “Z” (cyclonic)

“Z” = cyclonic flow in Central Europe on the 550 hPa geopotential level. Other option is “A” (anticyclonic)

“T” = air mass is dry (German *trocken*) with respect to the monthly mean precipitable water. Other option is “F”. i.e. The air mass is moist (German *feucht*) with respect to the monthly mean precipitable water.

## Comparison of the three classification schemes

Figure S1 gives absolute frequencies of the air mass categories for the three classification schemes. It can be seen that HBGWL and WLKC09 feature many categories that occur only seldom, even over climatologically relevant periods while BCLM provides less overall categories that occur at more balanced relative frequencies.

Figure S2 provides classifications of the dry scattering coefficient  $\sigma_{sc}$  at 550 nm, as an illustrative example. Mean values and standard deviation of  $\sigma_{sc}$  are given for each of the three classification schemes. It can be seen that BCLM turns out to be the scheme with the highest predictive power. In this context, “predictive power” implies that a classification segregates high and low values of a given parameter on a statistical basis efficiently.

Concretely, BCLM (13 categories) predicts a spread of  $\sigma_{sc}$  between 0.22 and 1.9  $\text{m}^{-1}$  depending on air mass type. This corresponds to a factor of 8.4. HBGWL (29 categories) predicts a maximum spread between 0.24 and 1.5  $\text{m}^{-1}$  corresponding to a factor of 6.2. WLKC09 (40 categories), at last, predicts a spread between 0.29 and 1.2  $\text{m}^{-1}$  corresponding to a factor of 4.1. In short, BCLM has the highest predictive power.

The effectiveness of BCLM appears even more superior when considering that it requires only 13 categories. HBGWL and WLKC09 provide many more possible air mass type categories, but supply inferior predictive power. This is manifested in Figure S3, which displays mean values combined with the standard error of the dry scattering coefficient. Here, the greater sample number per category can be felt, making BCLM the apparently more reasonable classification.

We conclude that in the context of this work, BCLM is a classification scheme that is clearly superior to the two other schemes investigated. The reason might be that BCLM uses direct information on vertical stratification, which is of immediate relevance of aerosol measurements near the ground.

More extensive evaluations of these classifications schemes, however, are needed in the near future for other aerosol parameters.

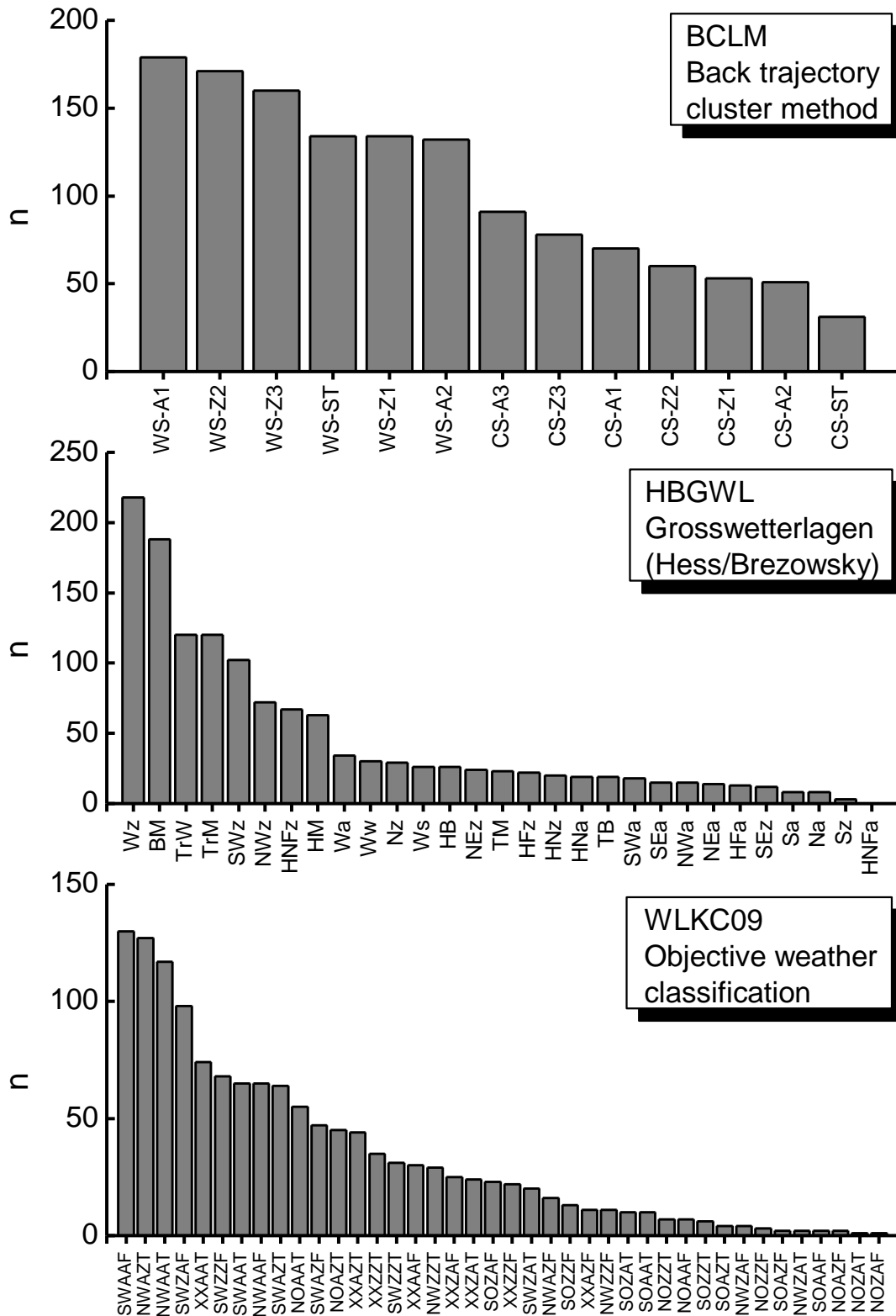


Figure S1: Absolute frequency of the air mass categories for the three classification schemes, 2007-2010. It can be seen that HBGWL and WLKC09 feature many categories that occur only seldom, even over climatologically relevant periods.

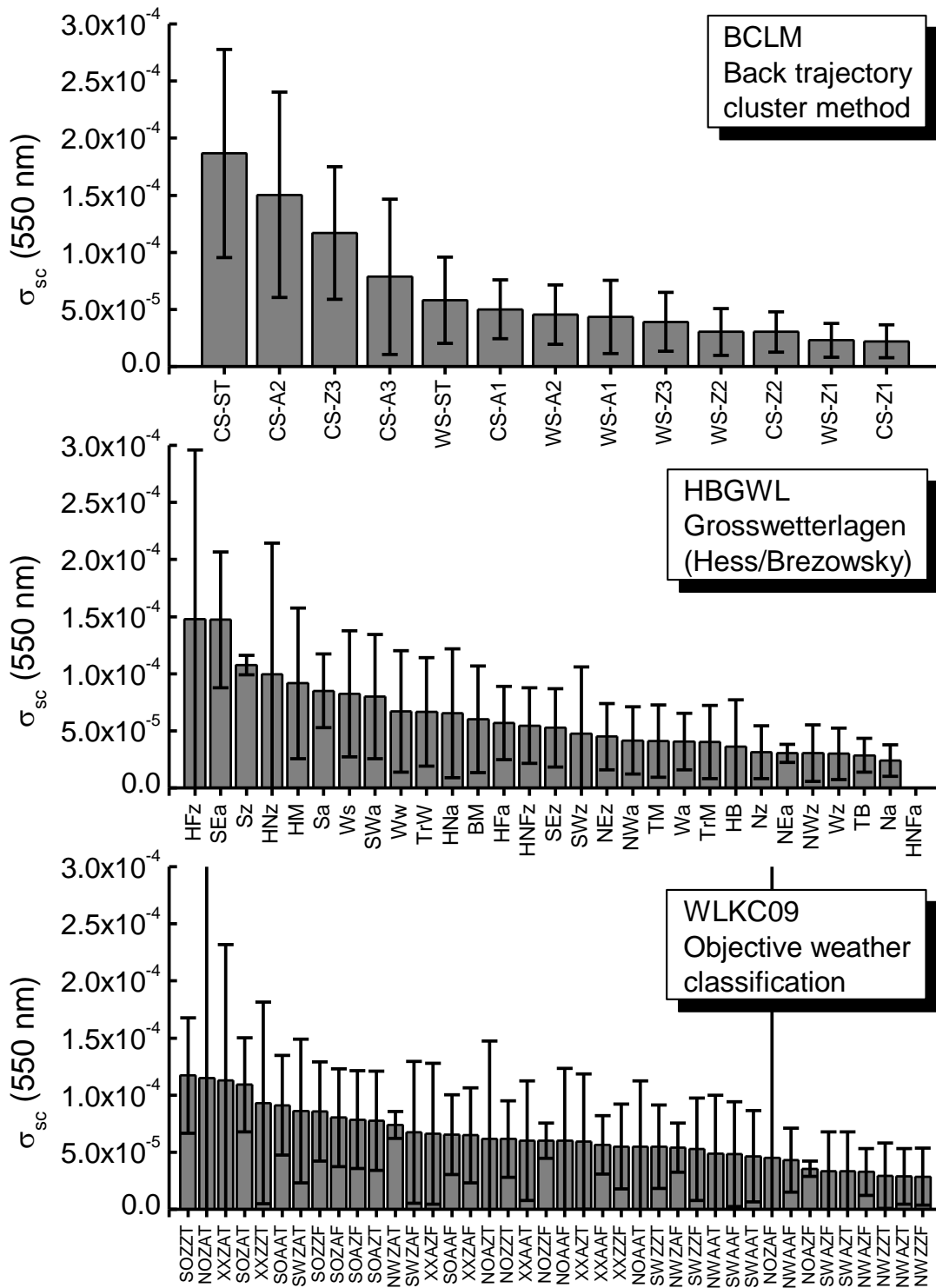


Figure S2: Mean values and standard deviation of the dry scattering coefficient at wavelength 550 nm ( $\sigma_{sc}$ ) in  $\text{m}^{-1}$ , 2007-2010. The diagrams are sorted after descending mean value per air mass type. It can be seen that BCLM is the most superior scheme to predict differences in  $\sigma_{sc}$ .

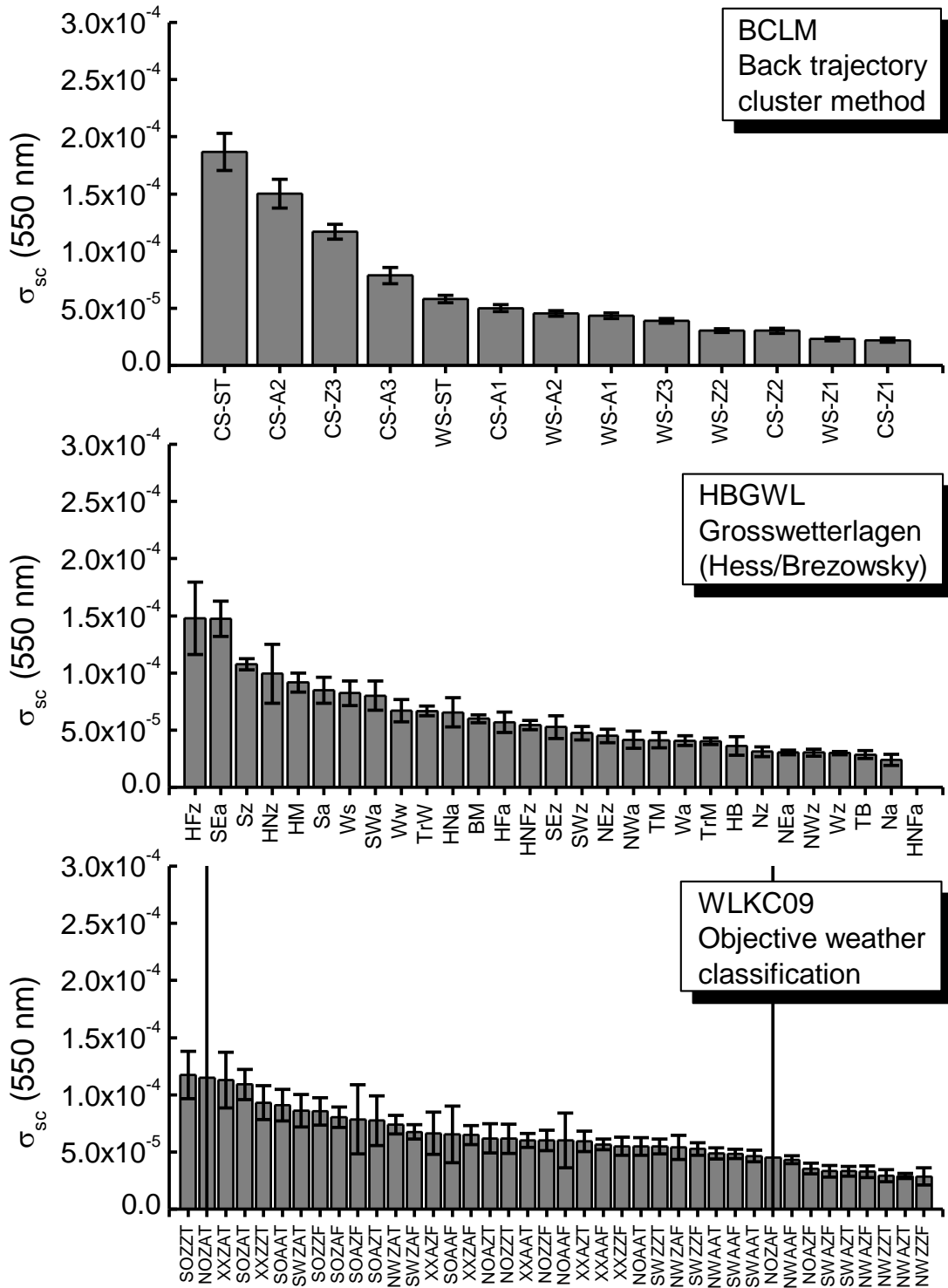


Figure S3: Mean values and standard error of the dry scattering coefficient at wavelength 550 nm ( $\sigma_{sc}$ ) in  $m^{-1}$ , 2007-2010. The diagrams are sorted after descending mean value per air mass type. It can be seen that BCLM is the most superior scheme to predict differences in  $\sigma_{sc}$ .

## References for this supplementary material

- Dittmann, E., Barth, S., Lang, J., Müller-Westermeier, G., 1995. Objektive Wetterlagenklassifikation (Objective weather type classification). Ber. Dt. Wetterd. 197, Offenbach a. M., Germany (in German).
- Gerstengarbe, F.-W. and Werner, P. C. (2005). Katalog der Großwetterlagen Europas (1881-2004) nach Paul Hess und Helmut Brezowski. Potsdam Institute for Climate Impact Research (PIK), Potsdam, Germany (in German).
- Hess P., Brezowsky, H., 1952. Katalog der Großwetterlagen Europas (Catalog of the European Large Scale Weather Types). Ber. Dt. Wetterd. in der US-Zone 33, Bad Kissingen, Germany (in German).
- James, P. M. (2007). An objective classification method for Hess and Brezowsky Grosswetterlagen over Europe. *Theoretical and Applied Climatology*, 88(1-2), 17-42.
- Philipp, A., Bartholy, J., Beck, C., Erpicum, M., Esteban, P., Fettweis, X. et al. (2010). Cost733cat–A database of weather and circulation type classifications. *Physics and Chemistry of the Earth, Parts A/B/C*, 35(9), 360-373.